Lab on a Chip

CRITICAL REVIEW

View Article Online
View Journal | View Issue

Cite this: *Lab Chip*, 2016, **16**, 2572

Oligonucleotide-based label-free detection with optical microresonators: strategies and challenges

Pelin Toren,[ab] Erol Ozgur[ab] and Mehmet Bayindir*[abc]

Received 19th April 2016,
Accepted 31st May 2016

DOI: 10.1039/c6lc00521g

www.rsc.org/loc

This review targets diversified oligonucleotide-based biodetection techniques, focusing on the use of microresonators of whispering gallery mode (WGM) type as optical biosensors mostly integrated with lab-on-a-chip systems. On-chip and microfluidics combined devices along with optical microresonators provide rapid, robust, reproducible and multiplexed biodetection abilities in considerably small volumes. We present a detailed overview of the studies conducted so far, including biodetection of various oligonucleotide biomarkers as well as deoxyribonucleic acids (DNAs), ribonucleic acids (RNAs) and proteins. We particularly advert to chemical surface modifications for specific and selective biosensing.

1. Introduction

Biosensing covers all the analytical methods used to detect the presence of biological entities within a medium and the interactions among them, using various equipment and methodologies. Besides its indispensable everyday applications, biosensing is also a prominent research field since there is a huge demand for label-free, ultra-sensitive, scaled down and robust biosensors in basic research as well as in the food, environmental, biomedical, and pharmaceutical technologies. For this purpose, during the past decade, a significant number of methods with novel alternative strategies[1–3] have been suggested.

Biosensors are analytical devices specialised for detection of a certain biological species. Similar to signal transduction pathways in cellular biology, biosensors consist of two basic parts, which are receptor and transducer. The receptor recognises the target, while the transducer converts the receptor–target interaction into a measurable signal. In biosensors, several transduction mechanisms exist, which can be categorised under main titles including mechanical,[4] acoustic,[5] electrical[6] and optical.[7]

Optical sensors, among the most investigated biosensing tools, particularly provide opportunities for label-free, highly sensitive sensing capabilities with small working volumes, easy on-chip integrations, and fast and multiple read-outs. They are also quite suitable platforms for investigating light–matter interactions. Since such interactions can be mathematically described using two parameters, refractive index (n) and extinction coefficient (k), these parameters also define the characteristics of materials in terms of optical properties. Therefore, a considerable amount of research has been devoted to deciphering and engineering the optical characteristics of materials. One of the important branches, which sprouted out of optical engineering, is detecting the presence of various interactions between materials by exploiting the changes in the measured optical characteristics.[8] Among different applications of optical detectors, one of the most practical applications is biological sensing, where optics provides invaluable opportunities.[9]

Most biological entities and biological interactions occur within the nanometer scale. This makes their direct visualisation impossible without causing them serious harm. Labelling biological samples with fluorophores is a limited solution with several issues to consider such as adverse interaction of the label with the sample and difficulty in real-time observation.[10] Therefore, label-free biosensors enabling detection of biological materials and their interactions are essential for a better comprehension of all biological phenomena. There are various methods for label-free biodetection,[11,12] all employing indirect methods for realising their purpose. Electrochemical sensors,[13] for instance, can measure a change in electrical impedance, conductivity or electric potential caused by the interaction of an analyte with the biosensor. Optical biosensors, on the other hand, provide this information by taking into account the changes in n and k using various strategies. Different types of biosensors possess distinct comparative advantages and deficiencies. These criteria directly influence their applicability over various biosensing issues. The most important characteristics determining the applicability of a biosensor are sensitivity, selectivity, dynamic range, robustness, and

[a] *Institute of Materials Science and Nanotechnology, Bilkent University, 06800 Ankara, Turkey. E-mail: bayindir@nano.org.tr; Tel: +90 312 290 3500*
[b] *UNAM-National Nanotechnology Research Center, Bilkent University, 06800 Ankara, Turkey*
[c] *Department of Physics, Bilkent University, 06800 Ankara, Turkey*

cost. These parameters are all intertwined, imposing strict compromises among each other.

Optical biosensors, compared to their mainstream biochemical or electrochemical counterparts such as Enzyme-Linked Immunosorbent Assay (ELISA)[14] or blood glucose sensors,[15] have a limited use in biosensing, particularly due to their generally complex operation and relatively higher performance and maintenance cost. On the other hand, there are certain potentials yet to be realised, motivating researchers to devote considerable effort in order to devise novel optical biosensors. The main reasons for pursuing optical sensors for the detection of biomolecular species and interactions are the possibility of ultimate, *i.e.* single entity, detection,[16] the potential of fabrication from well-defined materials,[17] and the maturity in methods for appropriate functionalisation of particularly silicon-based optical biodetection.[18]

Among various methods of optical biosensing, resonators of whispering gallery mode (WGM) type solely have the potential for ultimate sensitivity.[16] The WGMs were first observed in the inner walls of a cathedral with a circular structure, which allows sound waves to travel at certain frequencies through the inner circumference. Later on, a similar phenomenon was discovered in micro-optical structures, in which the light waves travel through a circular path due to total internal reflection.[16] In such structures, the resonant modes exist only at discrete multiples of wavelengths which are determined by the length of the resonators ($m\lambda = Ln$).[19] When an analyte is adsorbed on the microresonator surface, the path length of the light inside the microresonator is altered, causing a shift in the resonant wavelength, which is tracked for sensing and quantifying biological species.[20]

The figure of merit of these WGM microresonators is the quality (Q) factor, which is the ratio of the total optical power accumulated within the microresonator to the power dissipated with various mechanisms such as absorption, scattering or coupling.[21] The higher the Q factor of a microresonator, the sharper the resonant mode becomes due to the fact that the time each photon travels within the microresonator also increases while the circumference remains constant; thus, more strict measures apply for a photon to satisfy the resonance condition in terms of wavelength.[21] This positively affects the WGM biosensors in terms of sensitivity in two aspects, sharper resonances, which provide easier WGM shift tracking, and longer photon–analyte interaction times, thus increasing the efficiency. The latter one leads to one of the critical advantages of WGM biosensing, paving the way for single biological entity detection.[21] The only alternative to this strategy is reducing the mode volume, *i.e.* the volume in which light is confined drastically, such as in the case of plasmonic nanoparticles, where even alterations caused by single molecules become detectable.[22] Yet, compared to WGM biosensors, this is a relatively recent technology requiring a specialised set-up for dark-field imaging with high sensitivity. WGM microresonators have been recently demonstrated to be even capable of single molecule detection by exploiting the plasmonic enhancement.[23]

WGM biosensors form a suitable platform for biodetection in which light interacts with the analyte in the vicinity of the microresonator. In order to perform biosensing, light must be coupled to the microcavity during its travel. The most efficient method for coupling light by satisfying resonance conditions and observing a shift in the tracked resonance mode simultaneously is using a tuneable laser with a narrow linewidth. External cavity lasers[24] or distributed feedback lasers[25] are generally used for this purpose. Current laser systems provide tuneability with sub-picometer resolution. A significant part of biodetection using WGM microresonators is the detection of the optical signal. On this side, blind photodetectors connected to a power meter or directly to an oscilloscope could be effectively used.[26] The rest of the measurement is basically signal acquisition and processing, where an oscilloscope and a computer are required. A schematic description of WGM biosensing is given in Fig. 1.

WGM biosensors are mostly fabricated using standard micro-processing materials, *i.e.* silicon and silicon dioxide, *via* various microfabrication techniques. For producing some of the types including microtoroids, a post-fabrication process is required, in which surface roughness is significantly decreased by thermal treatment, resulting in ultrahigh Q microresonators, where energy dissipation primarily occurs due to optical absorption of the material from which the resonator is produced. These microcavities are referred to as surface tension induced microcavities (STIMs).[27] They have quite low surface roughness values, reducing scattering losses virtually down to zero. On the other hand, it is extremely cumbersome, if not impossible, to provide a robust on-chip waveguide integration with the STIM microresonators, except for some rare examples.[28] The light is commonly coupled to the STIMs either *via* tapered fibres or *via* prism couplers. However, these light coupling approaches require precise alignment and are inconvenient to integrate with microfluidic systems, particularly for the tapered fibre coupling. Non-STIM microcavities, on the other hand, can be fabricated with on-chip waveguides. However, they have at least 2 orders of magnitude lower Q values, preventing their use in single molecule biodetection.[21] Nevertheless, the non-STIM microresonators, particularly microrings, are significantly advantageous especially in multiplexed detection because tens of microrings can be fabricated and utilised in a parallel manner, and this is unique to the microring resonators.

Biosensing heavily depends on the sensitive and selective target detection capability of the biosensor. For this issue, the approach used in surface modification for conjugating probe molecules is crucial. In order to perform feasible biosensing, the surface of the biosensor should be engineered elaborately. Entities for molecular recognition, which are generally referred to as probe molecules, are a must for biodetection. The first prerequisite of the surface modification is covalent or non-covalent attachment of the probe molecules onto the biosensor surface. However, many parameters should be individually considered besides probe conjugation

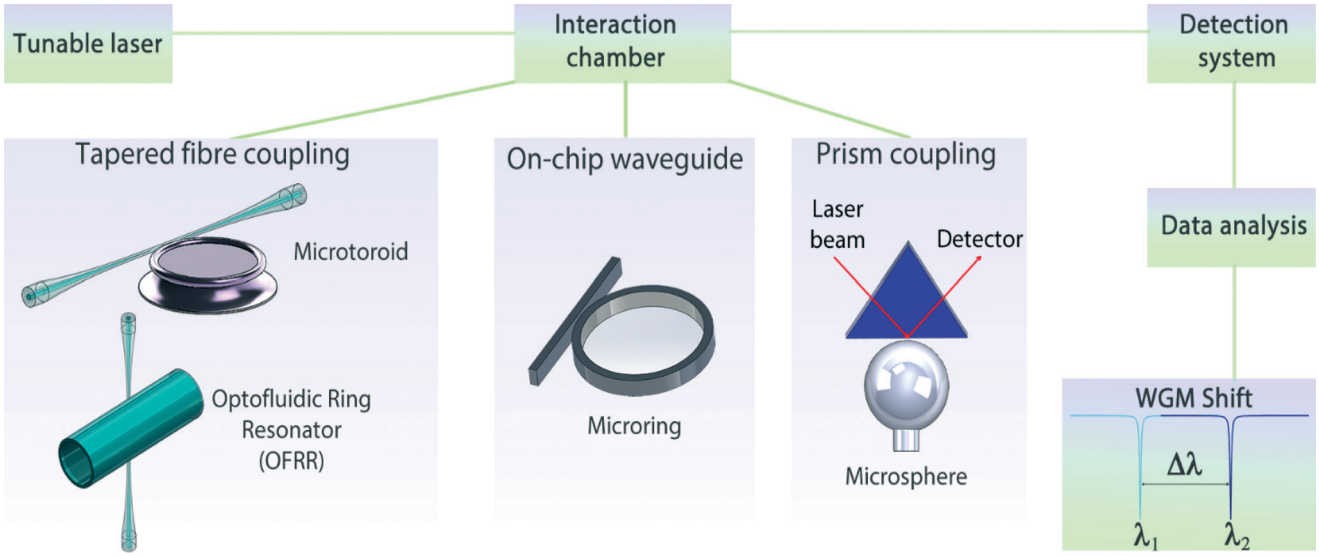

Fig. 1 Schematic diagram summarising the oligonucleotide-based biosensing approaches using various optical resonators (microtoroids, optofluidic ring resonators (OFRRs), microrings and microspheres). Light incoming from a continuously sweeping laser source is coupled to an optical resonator *via* a tapered fibre, an on-chip waveguide or a prism coupler. The intensity of the transmitted light is traced using a detection system. The resonance wavelength shift (from λ_1 to λ_2) of the traced WGM is analysed. The biosensing module, in which coupling and analyte infusion through the surface modified resonator occur, can be either a microfluidic or a flow system.

for an enhanced sensitive and selective biodetection. The approach used in probe conjugation can be considered adequate for a reliable biosensing to some extent; however, for most cases, additional surface chemistry is required, especially for biosensing in a complex medium.[26] A myriad of different strategies exist for biosensor surface modification, where different problems demand different solutions.[18] Yet, some of these solutions are inevitably more effective than those of their counterparts in terms of efficiency and reliability. Here, it is important to mention that silane-based surface modification is dominant in optical biosensors, since silane molecules enable covalent attachment on silicon/silica-based surfaces, which constitute the vast majority of the WGM biosensors. On the surface of a WGM biosensor, various functional groups can be obtained using silane chemistry. Each functional group provides a distinct characteristic to the biosensing system, while the strategy follows a common pattern based on silane chemistry, as illustrated in Fig. 2.[18] Adverting to surface modification strategies used in WGM biosensing is among the goals of this review.

Biomolecular interactions (such as antibody–antigen) occur within an aqueous medium. This fact compromises the use of the WGM type of microcavities regarding several aspects. The first issue that needs to be considered is the wavelength to be used. Although the optimum wavelengths in silica structures are 1310 and 1550 nm, which are also referred to as telecom wavelengths for the minimum loss of silica, at these wavelengths there is considerable water absorption.[29] Therefore, visible and near-infrared wavelengths, such as 670 nm, are shown to be more effective in optical biosensing.[29] Also, another important concern is optical coupling in aqueous media. Especially, tapered fibre coupling suffers heavily

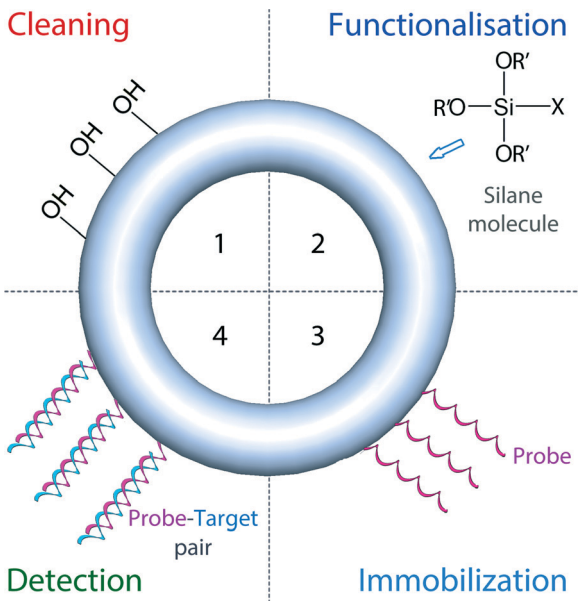

Fig. 2 Surface modification of an optical resonator for specific target detection. The schematic drawing shows a general approach to the chemical modification of a silicon/silica-based optical resonator for specific oligonucleotide-based detection. (1) Cleaning of biosensor *via* UV/ozone or chemical treatment to induce the formation of reactive silanol groups. (2) Pre-functionalisation of the biosensor surface with a silane molecule *via* silane condensation reaction, where OR′ can be a methoxy, ethoxy or acetoxy group and X can be an alkyl, aryl or organofunctional group. (3) Surface functionalisation by covalently conjugating an oligonucleotide probe (either modified or non-modified) to the silane-coated biosensor. Additionally, in between a silane molecule and a probe, a linker molecule can be used. (4) Specific target detection using probe–target interactions.

from mechanical perturbations occurring within the environment,[30] particularly by the presence of a fluid flow.

Microfluidic integration with the WGM biosensor increases the biosensing efficiency substantially. Yet, not all the optical biosensors, especially the high-*Q* ones, are compatible with microfluidic systems, mainly due to limitations in optical coupling. Microfluidic integration, on the other hand, provides invaluable efficiency and flexibility, especially in multiplexed detection. It would be fair to indicate that there is a trade-off between the sensitivity and the microfluidic compatibility of WGM biosensors, despite many serious efforts to overcome this challenge. For microresonators having a high-*Q* factor, an idealised multiplexed optical biosensing system with microfluidic integration is shown in Fig. 3.

The goal of this review is to discuss biodetection of/with oligonucleotides in detail. Oligonucleotide-based detection is a critical issue, since oligonucleotides possess the information regarding the origin and nature of life. Therefore, detection of oligonucleotides with high sensitivity and selectivity is an important issue accordingly. Among many different methods for oligonucleotide detection, quantification and analysis, optical biosensors are promising tools; yet, from our point of view, it is still far from realising their full potential.

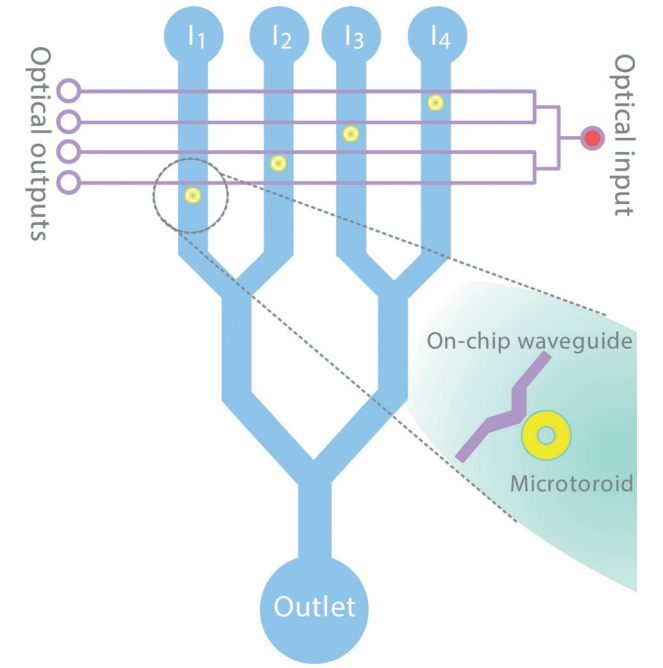

Fig. 3 Multiplexed oligonucleotide-based detection using microtoroids as optical resonators having high-*Q* factors. Illustration of a lab-on-a-chip biosensing system consisting of microfluidic channels each having one microtoroid (yellow circles), which can be used for multiplexed oligonucleotide-based detection. The proposed system has four inlets (from I_1 to I_4) and one outlet for controlled target flow in small volumes. Data are gathered separately from optical outputs, which are all branched from a common optical input (red lines). The inset shows an on-chip, curved waveguide and a microtoroid located at a critical distance as a schematic drawing regarding a previous work.[28]

Our aim for writing this review is therefore first critically analysing the current status of optical biosensing using particularly the WGM microresonators and then describing the pros and cons of each different approach within this broad set objectively. Finally, we would like to comment on the future direction of oligonucleotide-based optical biosensing. Also, significant attention to the surface chemistry used in WGM biosensors is required to understand specific molecular interactions.

This review is divided into three main sections according to target types (DNA, RNA and protein). Also, a comprehensive summary of different oligonucleotide detection strategies with their experimental results is given in Table 1. As can be seen from Table 1, there are already quite successful results in terms of sensitive and selective optical biodetection using oligonucleotides. Surface modification strategies using the WGM type of biosensors are considerably mature and serious progress has been made through optical coupling and microfluidic integration of these optical microstructures. Our primary aim is to explain the critical steps towards these accomplishments while writing this review.

2. Detection of deoxyribonucleic acid (DNA)

2.1 DNA hybridisation and distinguishing single mismatches

Since the identification of the structure of DNA[55] in 1953, at an increasing pace we are learning more about it. DNA molecules perform two important tasks: they replicate themselves by making copies of themselves from the beginning of life and they indirectly supervise the protein expression.[56] Thus, unsurprisingly, there is a tight relationship between various disease states and DNA alterations.[35] Understanding and detecting disease-related variations in DNA molecules are essential in early detection, which increases our chance of living.

There has been a tremendous effort to develop sensitive and sequence-specific DNA sensing platforms until now. Throughout the years, several DNA biosensing approaches have been developed, such as Polymerase Chain Reaction (PCR),[57] DNA arrays,[58,59] nanomechanical DNA sensors,[60] electrochemical DNA sensors,[61,62] and DNA biosensors based on graphene,[63] surface plasmon resonance,[64] nano-fibre[65] and nanowire.[66] Here, we introduce, DNA sensing approaches using optical microresonators.

It would be beneficial to begin with a former work of Vollmer F. and co-workers[31] in which multiplexed quantification of DNA was done using two silica microspheres. In order to hybridise with their fully complementary targets, individually, 27-mer oligonucleotides of interest were conjugated to dual microspheres *via* streptavidin–biotin interactions. By evanescently coupling light from a tuneable laser source to dual microspheres in a liquid sample cell, the resonances from each microsphere were identified separately in the transmission spectra as individual Lorentzian dips. In order to demonstrate the ability of the suggested biosensing platform in terms of distinguishing single mismatch alterations,

hybridisation between match and mismatch of an 11-mer oligonucleotide was shown. Also, the mismatch detection ability of the biosensor platform was demonstrated at an optimised specific temperature (~23 °C) and optimized salt concentration (20 mM tris, 30 mM sodium chloride at pH 7.8). The sensitivity of the suggested technique was reported as 6 pg mm^{-2} mass loading. The authors of the article provided information about the sensitivity of their biosensor only in terms of the mass loading, while the minimum detection capability according to the analyte concentration was not given.

A work of Wu Y. and co-workers[32] can be given as an example of the high specificity and sensitivity of DNA detection as an alternative approach besides its reusability and versatility. DNA loading and unloading from a microsphere (Fig. 4a) was provided *via* a DNA catalytic network scheme with a LOD of 22-mer DNA oligonucleotide of ~80 pM (32 fmol). Since the suggested idea was based on analyte unloading from the microresonator, a reusable DNA biosensor was obtained using this technology.

Probe DNA molecules, which could be used to detect multiple analytes, were attached to the microsphere surface *via* biotin–streptavidin interactions (Fig. 4b, P molecule) as in the previous study.[31] The DNA unloading from the surface occurred *via* a catalytic reaction (Fig. 4b, S and B leaves the surface). Fig. 4c shows the optical transmission spectra of the DNA unloading from the microsphere causing a blue shift. Single base alterations were reported, which were detected *via* the DNA loading/unloading rates by a factor of 40 to 100.

On the other hand, microrings as another branch of optical resonators are also opportune tools for DNA biosensing[33,67] and identifying the point mismatches[33,37,39] by providing high-throughput and real-time analyses with on-chip integrations as in arrays. In a work of A. J. Qavi and co-workers,[33] an isothermal approach to discriminate single nucleotide polymorphisms (SNPs) was demonstrated. 32 silicon microrings (30 μm in diameter) consisting of reference microrings for thermal drifts on a sensor array were assembled into a flow channel. *N*-Succinimidyl-4-formylbenzamide (S-4FB) modified ssDNA strands were covalently conjugated to HyNic silane functionalised microrings. Multiplexed DNA detection was provided by hand-spotting four different ssDNA probes having solutions complementary to 4 different target ssDNAs on a sensor array. Detection of the single base alterations was done by monitoring the desorption rates of the target ssDNAs leaving the formed DNA duplexes on the biosensor surface, similar to an approach demonstrated in the

Table 1 Comparison of oligonucleotide-based optical biodetection using the WGM type biosensors

Source	Microresonator type	Optical coupling	*Q* factor	Surface modification	Limit of detection (LOD)	Analyte introduction	Remarks
Single stranded DNA (ssDNA) detection							
Ref. 31	Microsphere	HF acid etched fibre	5×10^{5a}	Dextran + biotin/avidin	6 pg mm^{-2}	Fluidic	Two microspheres for multiplexed detection
Ref. 32	Microsphere	Tapered fibre	N/A[b]	Dextran + biotin/avidin	80 pM	Drop	Increased sensitivity with catalytic mass unloading
Ref. 33	Microring	On-chip waveguide	N/A	HyNic silane	1.95 nM (195 fmol)	Microfluidic	Multiplexed DNA detection
Ref. 34	Microtoroid	Tapered fibre	3.1×10^{7} and 4.6×10^{4a}	APTES/TMMS + EDC/NHS chemistry	2.32 nM	Fluidic	Single nucleotide DNA mutation distinguishability
Ref. 23	Microsphere	Prism	5×10^{6a}	CTAB stabilised gold nanorods	Single molecule	Fluidic	Plasmonic enhancement
Ref. 35	Microtoroid	Tapered fibre	2.2×10^{7a}	GPTMS	N/A	Fluidic	Fluorescence-based detection
Ref. 36	OFRR	Tapered fibre	10^{6}	3-APS + DMA as crosslinker	10 pM	Microfluidic	Interaction occurs in the fluidic core
Ref. 37	Microring	On-chip waveguide	N/A	APTES/GAD chemistry	25 nM	Drop	Detection in complex medium (human urine)
DNA amplification							
Ref. 38	Microring	On-chip waveguide	1.3×10^{4}	ABCR + click chemistry reaction	2 fg μl^{-1} (780 fM total DNA)	Microfluidic	Solid-phase recombinase polymerase amplification
Ref. 39	Microring	On-chip waveguide	N/A	APTES/GAD chemistry	500 fg μl^{-1} (80 nM total DNA)	Drop	Solid-phase recombinase polymerase amplification
Methylated DNA detection							
Ref. 40	Microring	On-chip waveguide	N/A	APTES/GAD chemistry	N/A	Drop	Two separately functionalized microrings for specificity
Ref. 41	Microring	On-chip waveguide	N/A	APTES/GAD chemistry	1% v/v methylated DNA	Microfluidic	Isothermal solid-phase amplification/detection
Ref. 42	Microring	On-chip waveguide	N/A	APTES/GAD chemistry	N/A	Microfluidic	Isothermal solid-phase amplification/detection, flexible device
Ref. 43	Microtoroid	Tapered fibre	2.5×10^{5a}	GPTMS	420 fM	Fluidic	Methylated cytosine-specific antibody as probe
Ref. 44	OFRR	Tapered fibre	N/A	3-APS + DMA as crosslinker	<1 nM	Microfluidic	MBD-2 protein as capture molecule

Table 1 *(continued)*

Source	Microresonator type	Optical coupling	*Q* factor	Surface modification	Limit of detection (LOD)	Analyte introduction	Remarks
Peptide nucleic acid (PNA) detection							
Ref. 45	Microring	On-chip waveguide	4×10^3[a]	APTES + SPDP as crosslinker	3 nM	N/A	Porous silicon for increased interaction area
MicroRNA (miRNA) detection and quantification							
Ref. 46	Microring	On-chip waveguide	N/A	APTES/S-HyNic silane	2 nM	Microfluidic	S-4FB modified capture probe
Ref. 47	Microring	On-chip waveguide	N/A	HyNic silane	10 pM (350 amol)	Microfluidic	S-4FB modified capture probe
Messenger RNA (mRNA) detection							
Ref. 48	Microring	On-chip waveguide	N/A	HyNic silane	512 amol	Microfluidic	DNA chaperones and beads for enhanced sensitivity
Transfer messenger RNA (tmRNA) detection							
Ref. 49	Microring	On-chip waveguide	N/A	HyNic silane	53 fmol ($\sim 3.16 \times 10^7$ CFU[c] of bacteria)	Microfluidic	DNA chaperones for disrupting secondary structure of tmRNAs
Aptamer-based protein detection							
Ref. 50	Microsphere	Fibre prism	N/A	3-APS + PDC as crosslinker	10 nM ($\sim$1 NIH[d] unit per ml)	Fluidic	Human thrombin detection
Ref. 51	Microring	On-chip waveguide	2.4×10^4	APTES/GAD chemistry	33 pM (IgE) and 1.4 nM (human thrombin)	Drop	IgE and human thrombin detection
Ref. 52	Microsphere	Tapered fibre	3.9×10^7 and 1.1×10^6[a]	MPTMS + disulfide coupling chemistry	$<$66 nM	Fluidic	Human thrombin and VEGF protein detection in human serum[e]
DNA–antibody conjugate for protein detection							
Ref. 53	Microring	On-chip waveguide	N/A	HyNic silane	N/A	Microfluidic	Alternative strategy for antibody conjugation

[a] *Q* value measured in aqueous environment. [b] Not available. [c] Colony forming units. [d] 1 NIH is equivalent to 1.1 to 1.3 international units (IU) thrombin.[54] [e] Diluted serum. Abbreviations: HF: hydrogen fluoride, HyNic: 3-*N*-((6-*N*′-isopropylidene hydrazino) nicotinamide) propyl triethoxy silane, APTES: 3-aminopropyltriethoxysilane, TMMS: trimethylmethoxysilane, EDC: 1-ethyl-3-(3-dimethylaminopropyl)carbodiimide, NHS: *N*-hydroxysuccinimide, CTAB: cethyltrimethyl ammonium bromide, GPTMS: 3-glycidoxypropylmethyldiethoxysilane,3-APS: 3-aminopropyltrimethoxysilane, DMA: dimethyl adipimidate, GAD: glutaraldehyde, ABCR: 11-azidoundecyl triethoxysilane, MBD-2: methyl binding protein, SPDP: succinimidyl 3-(2-pyridyldithio) propionate, S-HyNic: succinimidyl 5-hydrazinonicotinate acetone hydrazone, PDC: 1,4-phenylene diissothiocyanate, IgE: immunoglobulin E, MPTMS: 3-mercaptopropyl trimethoxy silane, VEGF: vascular endothelial growth factor.

aforementioned study[32] (Fig. 5a and b). The target binding kinetics due to either hybridising with fully complementary counterparts or targets having SNPs at different positions affected the desorption rates, resulting in different blue WGM shifts (Fig. 5c). The LOD for this study was reported as 195 fmol (1.95 nM) target DNA.

Nevertheless, single base pair alterations can also be observed using different approaches such as engineering the surface of the optical microresonators. Recently, we have demonstrated[34] how an optical microresonator with an engineered surface could be able to detect single base pair variations in a DNA molecule. Since detecting even point mismatches in the DNA molecule plays a vital role in DNA biosensors[31] in terms of enhancing the biosensor performance for distinguishing alterations, the suggested approach provided a considerably high selectivity for DNA biosensing.

Fig. 6a shows the SEM image of the fabricated microtoroid ($\sim$110 μm in diameter). The scheme for the surface engineering is shown step by step in Fig. 6b. For a selective single base pair DNA detection, the APTES and TMMS functionalised silica microtoroid surface was modified to obtain NHS esters *via* amine groups of the APTES molecules. While the amine groups were sequentially converted to carboxylates and NHS esters, the TMMS molecules remained the same on the surface and served as spacers to avoid steric effects which decrease the efficiency of the DNA hybridisation.[68,69] Covalent conjugation of the amino-modified ssDNA probes (Fig. 6b, red coils) was achieved *via* NHS-esters and the residual NHS esters were capped using ethanolamine, which resulted in a negatively charged microtoroid surface. Fig. 6c shows resonance wavelength shifts due to fully complementary (red data), point mismatched (blue data) and non-complementary ssDNA strands (grey data) of a 13-mer ssDNA probe in real time. Considerably late and slow responses were obtained from the point mismatch DNA and probe–DNA interactions as compared to the shifts (pm) observed in the complementary and probe–DNA interactions. Due to the fact that the surface had a negative overall charge, the repulsive forces occurring on the surface provided a high selectivity in terms of discriminating the single point alterations in *Pseudomonas aeruginosa* related oligonucleotide sequences. The LOD and surface coverage ratio of the captured targets to the attached probes were 2.32 nM and 0.84, respectively.

As one of the prominent examples of the optical microresonator-based DNA detection scheme, a work of M. D. Baaske and co-workers[23] can be given, in which they

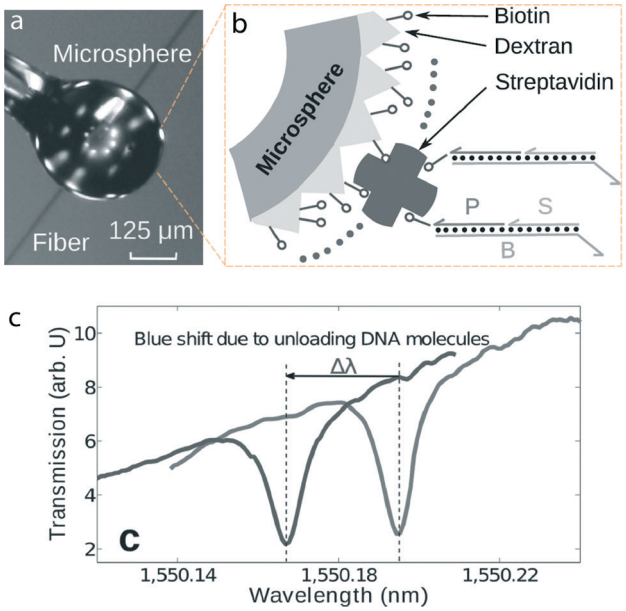

Fig. 4 DNA detection using a label-free microsphere integrated with a DNA catalytic network. (a) A micrograph of a microsphere (~300 μm in diameter), (b) the surface modification approach providing DNA loading/unloading (S and B molecules) with interaction with the DNA probe (P molecule) attached *via* biotin–streptavidin interactions, and (c) a blue WGM shift ($\Delta\lambda$) in the transmission spectra due to the loading and unloading of the DNA molecules in succession. Adapted from ref. 32 with permission.

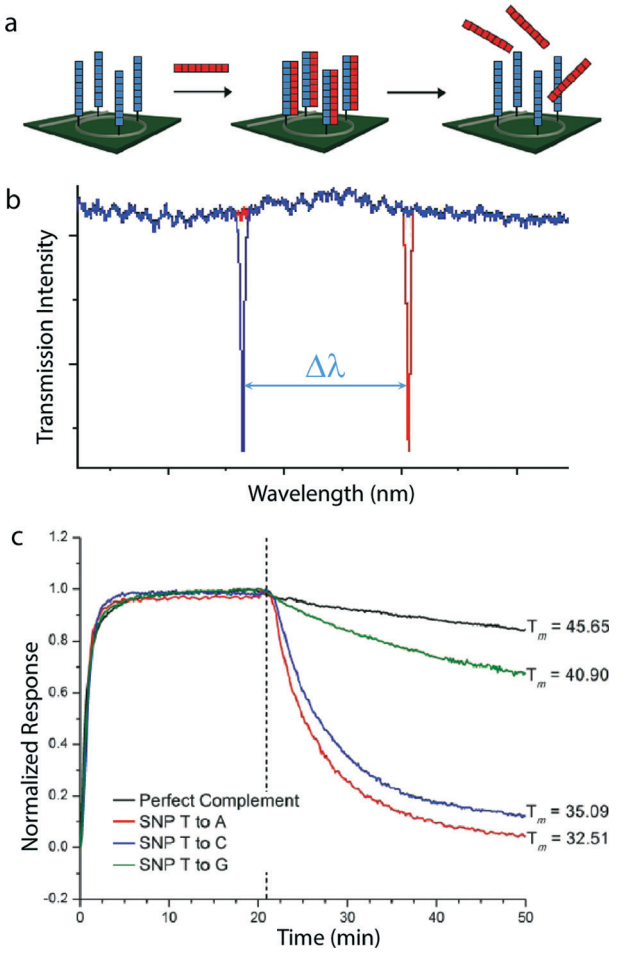

Fig. 5 Distinguishing the SNPs *via* real-time kinetic desorption using arrays of silicon microrings. (a) Schematic drawing showing hybridisation and dissociation between probe ssDNAs (blue strands) and complementary ssDNAs (red strands). (b) An observed blue WGM shift ($\Delta\lambda$) due to the desorption of the targets from the biosensor surface. (c) Hybridisation and desorption responses obtained from the ssDNA probe having microrings exposed to fully complementary counterparts and targets having SNPs at 3 different positions. Pure buffer was infused at time = 20 min. Adapted from ref. 33 with permission.

presented single nucleic acid detections using plasmonic nanorods adsorbed on silica microspheres (Fig. 7). Microspheres as optical resonators (Fig. 7a) are promising and sensitive tools for observing DNA–DNA interactions due to their high *Q* factors. However, lowering their detection limits down to single nucleic acids requires integration of the optical microresonators with plasmonic nanoparticles, which enhances the optical field strength at the microresonator surface.[23,70] Once the intensity of the surface plasmon resonance absorption increases, enhancement of the electric field is obtained. Gold and silver have a mean free path of ~50 nm, hence when their sizes are smaller than ~50 nm, only interactions with the surface are allowed since bulk interactions are not possible. The surface plasmon resonance condition is satisfied when the wavelength of light is much larger than the size of the nanoparticle and it depends on the size, shape and dielectric constants of the metal and surrounding material.[71] It was reported in the above-mentioned study[23] that gold nanorod (~12 nm × 12 nm × 42 nm) was chosen as the plasmonic nanoparticle because it provided strong field enhancements.

Thiol-functionalised oligonucleotides as receptors were covalently conjugated to CTAB stabilised gold nanorods following adsorption of the nanoparticles onto the microresonator surface. The optical measurements for observing nucleic acid kinetics were taken in a PDMS cell where target flow and the microsphere took place (Fig. 7b). The light from a continuously swept tuneable laser (~780 nm) was coupled to the microresonator *via* a prism coupler (Fig. 7b). It is noteworthy that the prism coupler is thoroughly helpful during the biosensing measurements as compared to the tapered optical fibres. It is important here to note that it is quite possible during a biosensing measurement, which is performed using a tapered fibre, to easily lose the transmission obtained from the fibre due to adsorption of the molecules in the tapered region, especially in concentrated measurement buffers. Another possibility, which is commonly encountered while using the tapered fibres, is that the changing coupling distance between the fibre and the microresonator can easily result in experimental errors. Such errors, for instance, can be avoided using UV-curable epoxy droplets by fixing the fibre from two sides.[34] However, fixing the fibre without losing the fibre transmission and breaking it is a challenging task. However, in the case of a prism coupler all these difficulties are avoided.

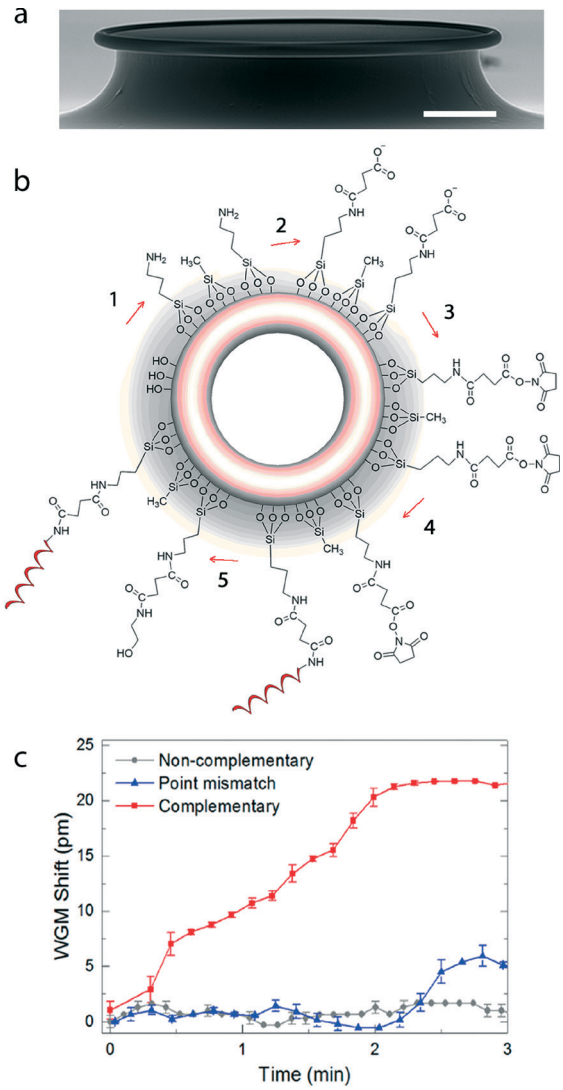

Fig. 6 Real-time and selective detection of single base pair alterations in the DNA molecules using surface engineered microtoroids. (a) Scanning Electron Microscopy (SEM) image of a fabricated microtoroid. (b) Step-by-step surface engineering of the microtoroid surface: APTES/TMMS silanization (1), succinic anhydride incubation in dimethylformamide (DMF) (2), EDC/NHS incubation in DMF to form NHS esters (3), ssDNA conjugation (red coils) to the formed NHS-esters (4) and capping of the residual NHS esters with ethanolamine (5). (c) Real-time WGM shifts (pm) due to fully complementary (red data), point mismatched (blue data) and non-complementary ssDNA strands (grey data) of the 13-mer ssDNA probe. Scale is 20 μm. Adapted from ref. 34 with permission.

Fig. 7c shows the monitored single DNA–DNA interaction kinetics in both the TE and the TM spectra simultaneously. A 22-mer oligonucleotide probe, interacting with its 3 base pair mismatched complementary target on the nanorod surface, caused resonance wavelength shifts ($\Delta\lambda$) in the fm level as spikes (Fig. 7c). Additionally, in this study, the detection of single interactions even down to octamers and small intercalating molecules was demonstrated. The suggested technique is also promising for biosensing applications integrated with microfluidic systems.

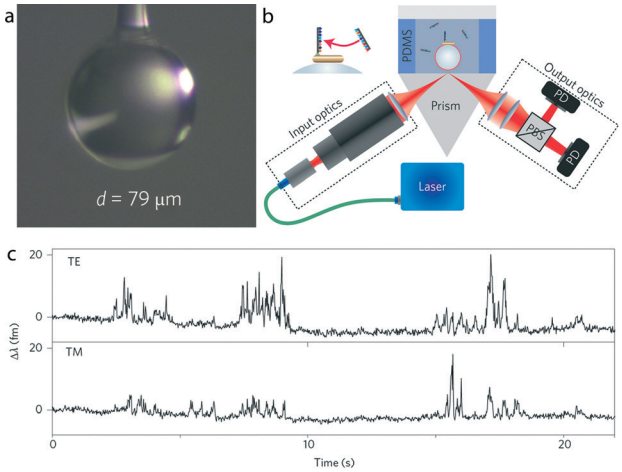

Fig. 7 Monitoring single molecule DNA interactions using a silica microsphere. (a) Image of a glass microsphere melted from an optical fibre (79 μm in diameter). (b) Schematic drawing showing oligonucleotide interactions on a plasmonic nanorod having a microsphere surface (on the top left corner) and biosensing set-up in which optical measurements were taken. A tuneable laser, centred at ~780 nm, was coupled to the microsphere in a polydimethlysiloxane (PDMS) cell *via* a prism coupler and transverse electric (TE) and transverse magnetic (TM) spectra were recorded using a polarising beam splitter (PBS) and photodetectors (PDs). (c) Recorded resonance wavelength shifts ($\Delta\lambda$) for TE and TM modes, simultaneously, due to interactions of 22-mer oligonucleotide probes with their three base pair mismatched complementary targets. Adapted from ref. 23 with permission.

An alternative approach for detecting formed DNA duplexes with microresonators was demonstrated in the work of R. M. Hawk and co-workers.[35] In this study, a microtoroid (Fig. 8a) was functionalised with GPTMS and then amino-

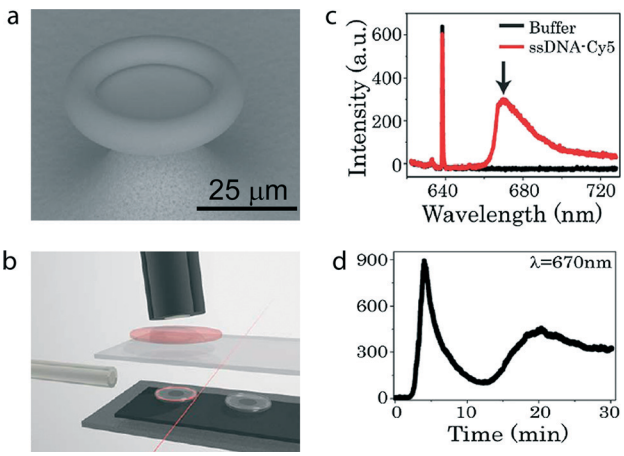

Fig. 8 Real-time and fluorescence detection of DNA hybridisation using a microtoroid with a functionalised surface. (a) Scanning electron micrograph of the fabricated microtoroid. (b) The biosensing set-up shows a fibre coupled spectrograph and a microtoroid. (c) The biosensor response to Cy5-labelled ssDNA targets is shown as a red line while the black line shows a case without the targets present. (d) The data show the response of the biosensor to unsuccessful (higher peak) and successful (lower peak) DNA hybridisations at 670 nm. Adapted from ref. 35 with permission.

modified 20-mer ssDNA probes were covalently conjugated to the microtoroid surface. The hybridisation between the probes and their cyanine (Cy5)-labelled counterparts was detected by a spectrograph (Fig. 8b). Fig. 8c shows the biosensor responses with and without 2 μM Cy5 labelled ssDNA targets present due to the excitement of the Cy5 fluorophore by the evanescent field. Fig. 8d shows transient and permanent peaks at 670 nm arising from unsuccessful and successful DNA hybridisations on the surface of the microtoroid, respectively. The study proposed a fluorescence-based DNA hybridisation technique in real time with detection of the target ssDNAs down to 1 nM.

Another approach for DNA sensing is through the use of OFRRs or liquid core optical ring resonators (LCORRs), which are suitable platforms for sensitive DNA detection and quantification.[72] The OFRRs offer ring resonator-based biosensing combined with microfluidics technology. The principle of the WGM-based DNA sensing using an OFRR is schematically shown in Fig. 9. A shift in the WGM mode can be observed with a refractive index change at near surface as the target ssDNAs hybridising with their probe counterparts attached on the inner surface of the OFRR during sample flow.

J. D. Suter and co-workers[36] used an OFRR or LCORR coupled to a tapered fibre (1550 nm) to show the DNA hybridisation with targets having different target lengths (25–100 bases) and the biosensor was able to distinguish base pair mismatches (from 1 to 5). The inner surface of the OFRR was modified with the 3-APS molecules and, using a homobifunctional linker DNA, amino modified ssDNA probes were covalently conjugated to the modified inner surface. The LOD of 25-mer DNA samples was given as 2.7×10^{10} molecules per cm^2. The mass loading limit of detection was reported in the order of 4 pg mm^{-2}, which was closer to the value obtained in the above study.[31]

Before concluding this section, we would like to advert to DNA detection in complex media using optical resonators. Biodetection in complex media is a challenging task since undesired non-specific interactions can easily occur between the biosensor surface and its surrounding medium, which results in false signals and compromises the selective detection of target molecules.[26] Y. Shin and co-workers[37] developed a biosensing platform consisting of an array of microrings (with a reference microring for the thermal drifts) for detection of DNA biomarkers related with bladder cancer in human urine (*mutated fibroblast growth factor receptor 3* and Harvey *RAS* genes). The DNA probes modified with an amine group were covalently attached to the APTES/GAD chemistry applied microring surfaces. An enhanced signal in the WGM shift was observed as the probe DNA molecules hybridised with their biomarker counterparts; however, the WGM shifts, due to the non-specific interactions between human urine and the microring surface, could not be eliminated and resulted in WGM shifts lower than the WGM shifts observed due to DNA hybridisation. While measuring in complex media, reducing the spectral shifts arising from non-specific interactions can only be achieved by using multifunctional surface modification, which enables probe conjugation and protein resistance simultaneously. In recent works,[26,73] we demonstrated a multifunctional surface coating which provides a selective biodetection of interleukin-2 antigens in complex media.

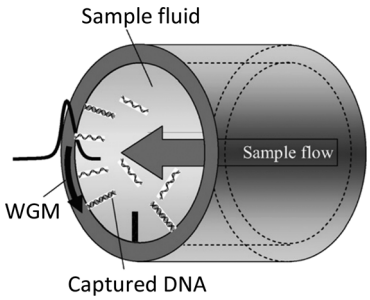

Fig. 9 An OFRR or a liquid core optical ring resonator (LCORR). WGM mode is supported within the circular cross section of the OFFR and evanescent sensing of the target ssDNAs occurs within the probe ssDNAs conjugated onto the hollow core during sample flow.[72] Adapted from ref. 36 with permission.

2.2 DNA amplification and detection of genetic variations

PCR[74] is the most commonly used nucleic acid amplification technique. However, recombinase polymerase amplification (RPA) is an alternative method to the PCR, which enables DNA amplifications at a low and constant temperature (~37 °C)[75,76] contrariwise to the PCR. This isothermal method provides enzyme-oriented synthesis[77] of the DNA molecules. Also, undesired side products of the PCR, such as primer dimers, can be reduced by using the RPA technique.[39] In a consecutive manner, the RPA process is performed by three enzymes: recombinase, ssDNA binding protein and polymerase. The recombinase forms a complex in between a template double stranded DNA (dsDNA) and its opposing primer parts and expedites the strand exchange at cognate sites (Fig. 10, (1) and (2)). Stabilisation of the structures is done by the ssDNA binding proteins which prevent branch migration[75] (Fig. 10, (3) and (4)). Lastly, DNA elongation is performed by the strand displacing polymerase to end the RPA process (Fig. 10, (4) and (5)).

Combining the RPA technique in the solid-phase with an optical microresonator having a biosensor array is an emerging field, which enables real-time and specific DNA detection by providing rapid DNA amplification in a small working volume. For this purpose, J. S. del Rio and co-workers[38] developed a biosensor platform consisting of arrays of label-free microrings to perform solid-phase RPA (SP-RPA) of the DNA molecules.

As shown in Fig. 11a, the fabricated biosensor chip had 8 columns of 4 pairs of microrings. 4 microfluidic channels having 6 pairs of functionalised and 2 pairs of non-functionalised microrings as blank controls addressed a total of 8 pairs on the biosensor chip. Collected light at input optical couplers was directed through waveguides in order to be

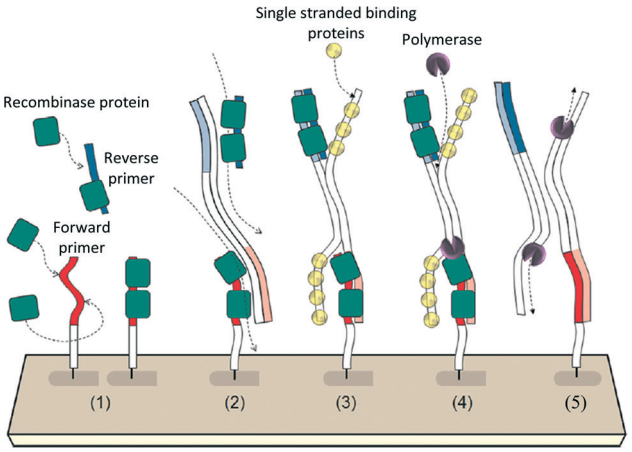

Fig. 10 The RPA process in the solid phase. The recombinase proteins form a complex between forward/reverse primers and the template dsDNA (1), the recombinase proteins scan the dsDNA for cognate sites (2), strand displacement occurs while the structures are stabilised by ssDNA binding proteins (3), and DNA amplification is done by polymerase ((4) and (5)). Adapted from ref. 38 with permission.

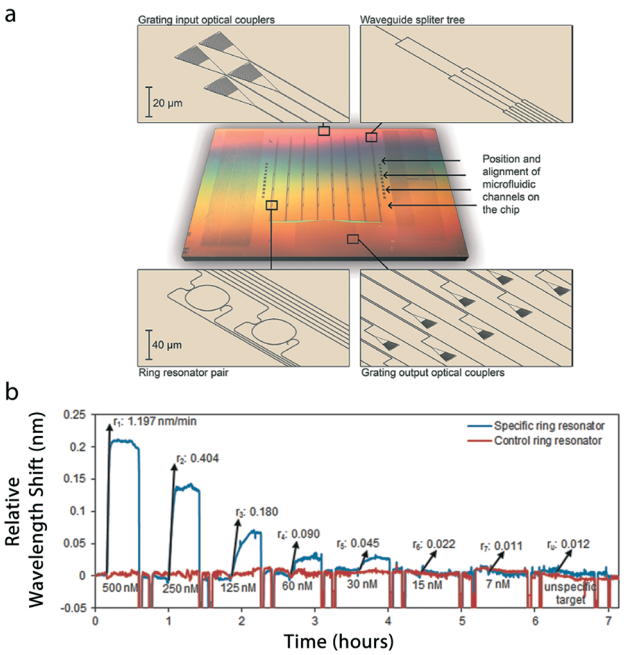

Fig. 11 The SP-RPA of DNA using label-free microring arrays. (a) Schematic drawing of the biosensor chip having arrays of microrings (8 columns of 4 pairs). (b) Real-time, relative wavelength shifts (nm) due to hybridisation of 25-mer ssDNA at different concentrations (blue data) and the sensor response of the reference microrings (red data). The magnitudes of initial transient slopes are given in nm min^{-1}, indicated with an arrow. The decay in the wavelength shifts was observed due to regeneration of the probes. Adapted from ref. 38 with permission.

coupled to the microrings, and the resonance wavelength shift data was gathered from output optical couplers. To functionalise the surface, covalent conjugation of hexynyl terminated ssDNA probes to ABCR modified microrings was achieved *via* a click chemistry reaction. Detection of pathogen *Francisella tularensis* related dsDNA was done with the microrings having *F. tularensis* forward primers.

Fig. 11b shows responses of the microrings to different analyte concentrations due to hybridisation of 25-mer ssDNA targets. Two representative microrings showed significant responses to the target ssDNA infusion. The functionalised microring (blue data) for a specific ssDNA detection revealed significant wavelength shifts while the control microring (red data), functionalised with a poly30T back filler, showed responses only in the order of background noise to varied concentrations of the ssDNA target solution. Also, the biosensor showed no significant response to unspecific ssDNA targets, proving the ability of the biosensor in terms of selectivity. Withal, the method suggested a rapid DNA amplification time (40 min) with a low LOD (2 fg μl^{-1}) level while the LODs in the standard RPA and the conventional/real-time PCR techniques were reported in the order of pg μl^{-1} levels.[38,39]

Y. Shin and co-workers[39] suggested a label-free, multiplexed DNA amplification platform with faster times (20–30 min) as compared to the above study. In order to detect single point mutations in the Harvey RAS (*HRAS*) gene, they fabricated an isothermal solid-phase amplification/detection (ISAD) device consisting of APTES/GAD chemistry applied microrings. The LOD was reported as 500 fg μl^{-1} for this study.

2.3 Detecting methylated DNA and its oxidised derivative

DNA methylation is an epigenetic modification which results in a 5-methylcytosine (5mC) molecule *via* covalent modification of the fifth carbon in the DNA base cytosine (Fig. 12a and b).[78] The DNA methylation can be presented in CG, CHG and CHH sequences where H can be A, T or C.[79] Without any sequence change, *via* a chemical modification, DNA methylation can alter the function of the DNA molecule. For instance, it has been revealed that DNA methylation plays essential roles in various cellular processes[80] such as development and regulation in gene expression (*i.e.*, gene silencing in eukaryotic cells).[79,81–84] Expectedly, abnormal methylation processes occurring in the chemical structure of the DNA molecule have a relationship with numerous diseases.[80,85] Recent studies have also shown that oxidation of the 5mCs by enzymes like human ten-eleven translocation 1 (*TET1*)[86] leads to 5mC derivatives such as 5-hydroxymethylcytosine (5hmC) which was first found in mammalian genomic DNA[87] in 1972.[88] Like the 5mCs, the 5hmCs are also known to be involved in embryonic development as well as many diseases.[84] Additionally, methylated DNA molecules are also known as biomarkers for cancer.[89]

Bisulfite sequencing is the most widely used method for analysing DNA methylation by converting non-methylated cytosines to uracils selectively while keeping methylated cytosines unchanged.[42,90,91] Among techniques based on bisulfite conversion for methylated DNA detection, methylation-specific (MS) PCR[92] is the most commonly used method.[41] Despite the fact that MS PCR is widely used, alternative

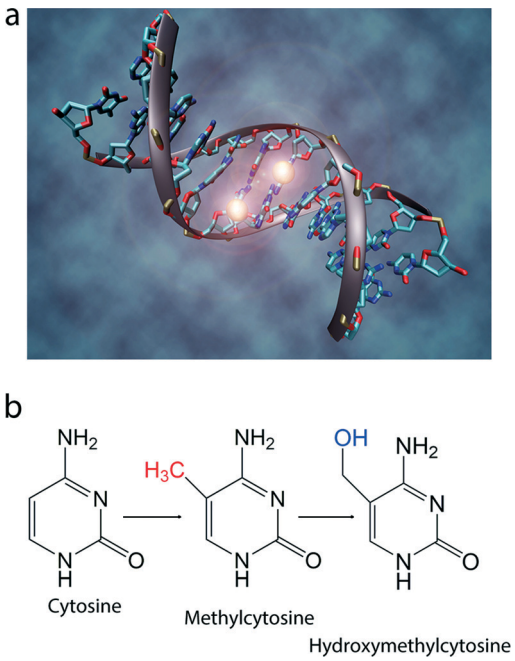

Fig. 12 Chemical modification of a DNA molecule by methylation *via* cytosines. (a) The illustrative image shows the crystal structure of a methylated DNA double helix (with sequence ACCGC**CG**GCGCC) at two reciprocal central cytosines (illustrated by Christoph Bock, Max Planck Institute for Computer Science, Computational Biology and Applied Algorithms). (b) Chemical structures of the cytosine, methylcytosine and hdroxymethylcytosine molecules.

detection techniques have also been suggested due to the complexity and long analysis time of the MS PCR.[41,42] For instance, Y. Shin and co-workers[40] showed the detection of DNA methylation biomarkers, *RARβ* (Retinoic acid receptor β),[93–95] *DAPK* (Death-associated protein kinase)[96,97] and *E-cadherin* (epithelial cadherin)[93,98] genes since their included DNA methylation patterns are well known in human cancer including bladder cancer. Microring arrays, each containing 4 rings (3 measurement rings and 1 reference ring to control thermal drifts), were fabricated for this purpose. Probes having either methylated cytosine or unmethylated thymine were covalently conjugated to APTES/GAD chemistry applied microrings. Using the surface modified microresonators provided real-time analysis and discrimination of methylated and unmethylated DNA targets following the bisulfite conversion of the targets. However, as the authors also indicated, for such an approach, a compact biosensor chip having microfluidic channels and sequential process steps were required to reduce the process time.

Later on, J. Yoon and co-workers[41] suggested a practical on-chip platform to analyse the methylation status of DNA in real time based on the former approach.[40] Fig. 13a shows the fabricated biosensor chip consisting of a pre-processing module for the bisulfite conversion (red micro-channels) and a detection module for analysis of the DNA methylation (blue micro-channels). The methylation status of DNA, obtained from a cancer-related epithelial cell line (*RARβ*[93–95] gene as a common human DNA methylation biomarker), was detected

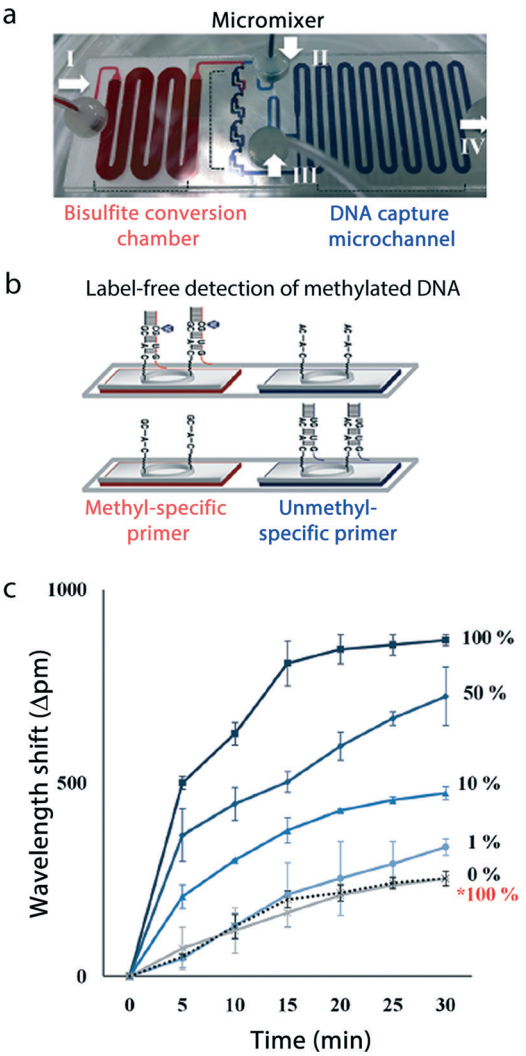

Fig. 13 On-chip device for real-time DNA methylation analysis. (a) Fabricated biosensor chip having a pre-processing chamber for bisulfite conversion (red micro-channels) and a detection chamber for the DNA methylation analysis (blue micro-channels) with three inlets (I, II and III) and an outlet (IV). (b) Detection of target DNA strands with methyl-specific or unmethyl-specific primer probe having microrings. (c) Response of the biosensor to the methylated DNA targets in different percentages ranging from 0% to 100% (data from light to dark blue). Also, the response of the biosensor having unmethyl-specific probes is given as a negative control (*100%). Adapted from ref. 41 with permission.

by methyl-specific or unmethyl-specific primers conjugated to biosensor chips following the bisulfite conversion of the DNA targets (Fig. 13b). The suggested idea provided amplification of the methylated DNA strands and specific detection down to 0% in terms of target concentration (Fig. 13c, blue data varying from light to dark blue) in a mixture containing methylated and unmethylated DNA strands. The response of the biosensor system showed a significant non-specific resonant wavelength shift, probably due to relatively poor discrimination of the used DNA probes against the targets.

As a similar approach to the former work,[41] T. Y. Lee and co-workers[42] developed a flexible and on-chip biosensing

platform for detection of the methylation status of the *RARβ*[93–95] or *HAAO* (3-hydroxyanthranilate-3,4-dioxygenase)[99] genes as other cancer biomarkers within 65 min. In this work, instead of the bisulfite conversion, methylation specific endonuclease digestion[100] was used. Additionally, the fabricated biosensor chip consisted of two parts: a modification module in which cleavage of the appropriate sequence sites (CCGG) by the enzymes occurred, and a detection module to understand the methylation status of the targets.

In order to detect the oxidised derivative (5hmC) of the 5mC molecule, R. M. Hawk and co-workers[43] used microtoroids (Fig. 14a) for selective detection of 5mC and 5hmC molecules. In this regard, the anti-5hmCs were covalently conjugated to a GPTMS-coated microtoroid. The measurements were taken in a sample chamber having a microtoroid and a tapered silica fibre (765 nm) in 100 μl ofphosphate buffered saline as the measurement solution. Fig. 14b shows the biosensor response to 50 μl min^{-1} injection of different oligonucleotide targets in varying concentrations. As shown in Fig. 14b, a significant WGM shift was observed due to the 5hmC infusion while lower shifts were also observed in unmethylated cytosine (C) and the 5mC infusions due to possible non-specific binding interactions between the biosensor surface and the targets. The LOD for this study was reported as 4.2×10^{-13} M with a detection of the 5hmC signal, which was twice that of the 5mC signal.

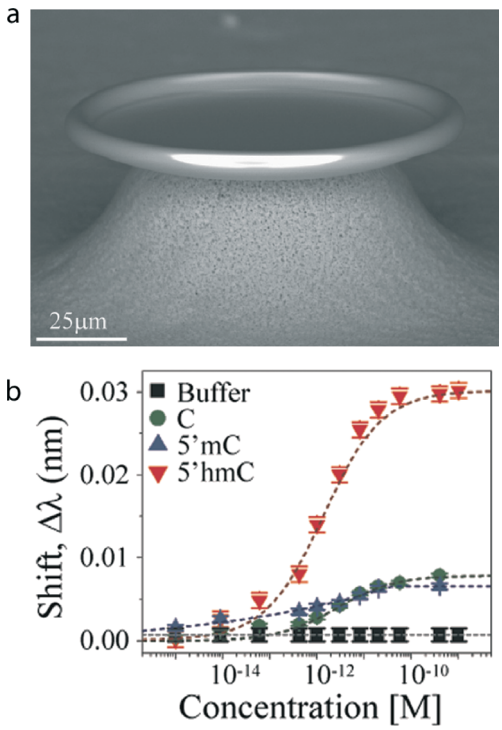

Fig. 14 Detection of the 5mC and 5hmC molecules using 5hmC antibody (anti-5hmCs) conjugated microtoroids. (a) Scanning electron micrograph of a fabricated microtoroid. (b) The response of the biosensor to buffer, unmethylated (C), methylated (5mC) and hydroxymethylated (5hmC) cytosine solutions in varying concentrations (from 1 fM to 1 nM) using a tuneable laser centred at 765 nm. Adapted from ref. 43 with permission.

The OFRRs are also functional platforms for DNA methylation analyses because they provide fluidic integrations. J. D. Suter and co-workers[44] used methyl binding protein (*MBD-2*) and 5-methylcytidine antibody as probe molecules to detect artificially methylated ssDNA and dsDNA molecules by OFRRs coupled to tapered fibres (1550 nm). Either the *MBD-2* or the anti-5-methylcytidine probes was covalently conjugated to a 3-APS-coated inner biosensor surface *via* DNA as a bifunctional linker. The suggested system was able to discriminate methylated and unmethylated DNA strands. They also reported strong binding affinities of dsDNA and ssDNA to the *MBD-2* and the 5-methylcytidine antibody, respectively.

2.4 Detecting peptide nucleic acid (PNA)

PNAs are artificially synthesized oligomers of peptides which have backbones analogous to the ones that nucleic acids have.[101,102] The PNAs are more resilient than the DNA probes towards degradation by enzymes, and they can be modified in order to capture DNA strands with high specificity and affinity.

In a recent work of G. A. Rodriguez and co-workers,[45] interaction between the PNAs and the DNAs was exploited using porous silicon (PSi) ring resonators in the biosensing applications. The fabricated Psi ring resonator coupled to its linear waveguide is shown in Fig. 15a. The PSi ring resonators enable a larger area of interaction for the target molecules with the sensor surface compared to the surface area limited detection using other types of sensors. The Psi structure was obtained *via* controlled electrochemical etching of silicon, and a refractive index alteration was created by partial thermal oxidation.

The whole surface of the PSi ring resonator was modified with APTES molecules and SPDP was used as a crosslinker to conjugate DNA probes for capturing target PNAs. As shown in Fig. 15b, WGM shifts were observed due to sequential attachment of the probe DNAs (100 μM) and target PNAs (500 nM) to the SPDP-modified PSi ring resonator surface. The probe DNA attachment to the SPDP-modified ring resonator surface caused a significant WGM shift due to the high probe concentration used. In addition, target PNAs hybridised with the probe DNAs led to an observable WGM shift of 11.10 nm.

Moreover, the *Q* factor of the fabricated PSi ring resonators in the buffer was reported to have an order of magnitude of 10,[4] while it was one order of magnitude higher in air. This is partially related to the wavelength of the laser (~1550 nm) used in this work, at which water absorption[29] in aqueous media cannot be neglected. Still, the authors reported that the sensitivity for PNA was 3 nM as calculated by 3σ analysis, while directly measured lower concentration was reported as 42 nM. Overall, the authors suggested that the sensitivity of porous silicon microrings could be engineered to be higher than that of the conventional silicon microrings. On the other hand, there are examples of the opposite case, where silicon microrings were shown to have similar

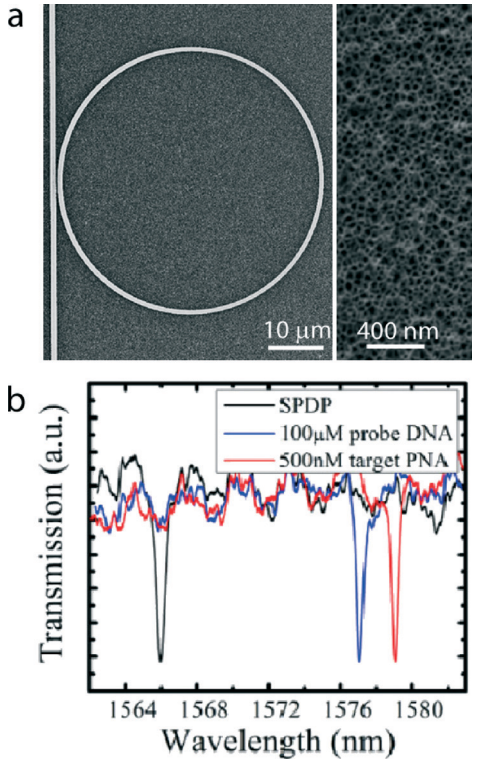

Fig. 15 The PSi ring resonator for biosensing applications. (a) An SEM image of the Psi ring resonator (left) with a zoomed image showing the porous structure (right). The porosity was attained by electrochemical methods, while a higher refractive index on the waveguide part was fabricated using thermal oxidation. The oxidised part was then further functionalised. (b) Shifts of the WGMs in the transmission spectra due to sequential attachment of the probe DNAs and the target PNAs to the SPDP functionalised PSi ring resonator. Adapted from ref. 45 with permission.

sensitivities towards oligonucleotides as well, as already mentioned in this review.[33,46]

3. Detection of ribonucleic acid (RNA)

3.1 Multiplexed microRNA (miRNA) detection and quantification

miRNA, which is a small RNA molecule (containing 19–24 nucleotides[46]) that does not encode proteins,[103] had been first identified as *lin-4* (ref. 104) in 1993. However, the function of the miRNAs as regulators was discovered in the early 2000s.[105–107] These tiny RNA molecules, since then, have been known to possess transcriptional and post-transcriptional roles in gene expression.[108] The discovery of the regulatory function of the miRNAs has led the way to gathering further knowledge on their roles in biological processes. For instance, miRNAs are known to play profound roles in cellular processes (such as proliferation,[109] apoptosis[110] and development[111]). Additionally, they also take part in various diseases such as cancer,[112] diabetes,[113] and cardiovascular,[114] autoimmune[115] and neurodegenerative[116] diseases. Thus, they are excellent biomarkers for the early detection, diagnosis and prognosis of a disease. Increased or decreased levels of miRNAs in cells can be indicators of many diseases.[117] Conventional techniques for miRNA detection can be listed as cloning,[118] Northern blotting,[119] reverse transcription polymerase chain reaction (RT-PCR)[120] and microarray[120,121] analyses. However, many of these techniques require a large amount of samples[46] and suffer from complexities.[47,122] F. Porichis and co-workers,[123] demonstrated miRNA detection using fluorescence *in situ* hybridisation (FISH) technique combined with flow cytometry. Recently, among label-free techniques,[124] electrical detection techniques[125] based on detecting a change in current due to hybridisation between miRNA and probe, and optical detection techniques[125] (label, label-free, spectroscopy and refractive index based) have been suggested to increase the sensitivity of the miRNA detection.

Among optical techniques, the detection of miRNAs using on-chip integrated microring optical resonators provides rapid, robust and multiplexed detections[126] with considerably high miRNA sensitivities.

There are two noteworthy examples[46,47] of miRNA detection which used microring optical resonators. A. J. Qavi and R. C. Bailey[46] reported a multiplexed miRNA detection platform using silicon photonic microring resonators. For this purpose, they fabricated sensor chips each containing 32 individual microrings including reference microrings having 30 μm diameter with its adjacent linear waveguide (Fig. 4a). This biosensing platform possessing multiple microrings with several unmodified microrings, which serve as references, is quite advantageous in terms of data corrections for undesired non-specific interactions and shifts due to thermal and instrumental fluctuations. For surface modification, the sensor chips were exposed to S-HyNic solution following APTES solution. ssDNA probes (22-mer nucleotides), which reacted with the S-4FB heterobifunctional crosslinker previously, were conjugated covalently to the modified sensor chip surface. A tuneable laser, centred at 1560 nm, was coupled to the linear, on-chip waveguides and a resonance wavelength was tracked. Target miRNA infusions to the sensor chips were performed in microfluidic flow channels.

Fig. 16b shows a schematic demonstration of hybridisation between target miRNAs (red) and probe ssDNAs (black) which leads to a significant shift (Δpm) in the tracked resonance wavelength. The applicability of the sensor chips to a multiplexed miRNA analysis is demonstrated in Fig. 16c. Four sets of microrings were functionalised with four different fully complementary ssDNA probes, individually. Each modified microring showed a dramatic response to its corresponding target miRNA during the sequential introduction of brain cancer relevant miRNA targets (miR-133b, miR-21, miR-24-1 and let-7c) through the microfluidic system. Although the miRNA targets had the same length (22-mer nucleotides), variations in the resonance shifts that were observed as they hybridised with their complete counterparts on the biosensor surface (Fig. 16c) remained as an unaddressed issue. In this study, a detection limit of 150 fmol of miRNA was reported and the suggested biosensing mechanism provided a multiplexed quantification of the 4 aforementioned miRNAs. Moreover, an isothermal method was suggested to discriminate single base

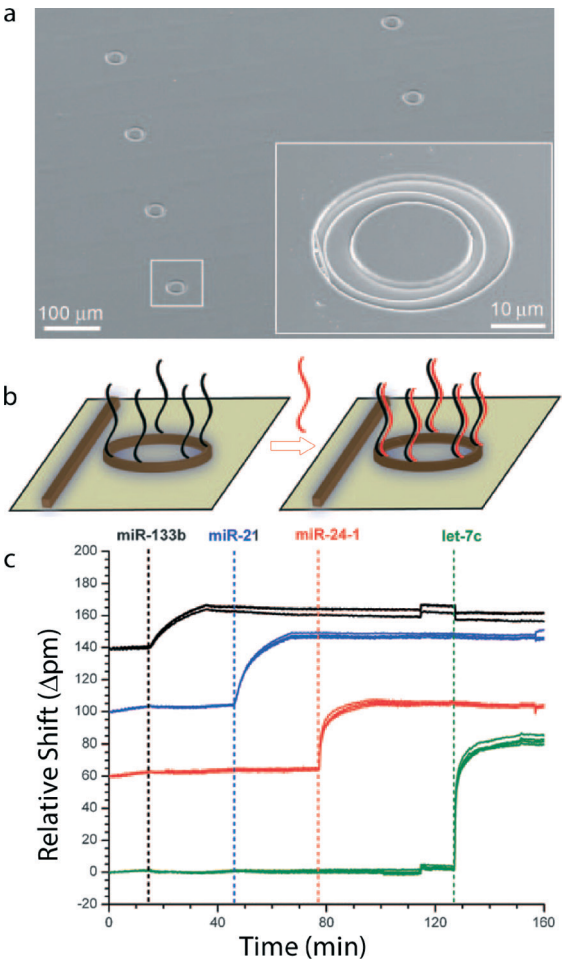

Fig. 16 Label-free and multiplexed detection of miRNAs. (a) Scanning electron micrograph of a microring with its linear waveguide (indicated with an arrow), (b) schematic drawing showing target miRNAs (red) captured by ssDNA probes (black) and (c) specific detection using four different miRNAs (miR-133b, miR-21, miR-24-1 and let-7c) on a single chip containing four sets of microrings, each functionalized with different ssDNA probes. In between each miRNA infusion, phosphate buffered saline solution was introduced to the system. Adapted from ref. 46 with permission.

differences by performing hybridisation in 50% v/v formamide solution. Since detecting single base pair variations in an oligonucleotide is a challenging task, the demonstrated miRNA biosensing platform suggests a highly sensitive and selective miRNA detection approach.

Another example of the multiplexed detection of miRNA is the other work of A. J. Qavi and co-workers.[47] They fabricated sensor substrates each containing 32 addressable microring resonators in the same manner as that in the previous works[33,46,126] and S-4FB modified ssDNA probes (22-mer nucleotides) were covalently conjugated to Hy-Nic silane-coated sensor substrates. An external cavity laser was used to trace the resonance wavelength. They fabricated laser etched microfluidic channels for analyte infusion.

Fig. 17a shows their miRNA sensing approach in this work. Target miRNAs were infused, using a peristaltic pump, through the microring having fully complementary ssDNAs. Subsequently, antibody S9.6 (anti-DNA) was harvested from a mouse hybridoma cell line that was able to recognise the formed DNA–RNA heteroduplexes on the surface and was introduced to the system following blocking of the microring surface to avoid non-specific interactions. As shown in Fig. 17b, resonance wavelength shifts (Δpm) for 3 separate microrings were observed after anti-DNA infusion following target miRNA infusion. Since anti-DNA binding response was higher than that of the bound miRNAs to the surface, the system provided an enhanced miRNA detection limit down to 350 amol (10 pM), which is lower than the detection limit reported in the previous study.[46]

In order to investigate antibody (S9.6) binding kinetics, antibody solutions having the same concentration (2 μg ml^{-1}) were infused to the microrings with varied capture probe

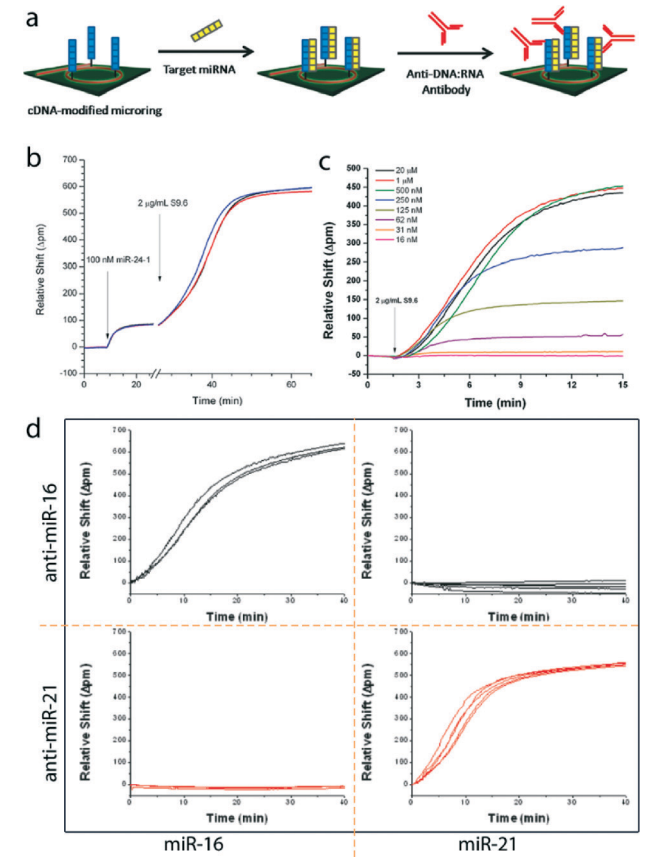

Fig. 17 Increasing sensitivity in silicon photonic microring resonators using antibodies. (a) Schematic drawing showing DNA probe modified microring exposed to target miRNA and antibody (S9.6) sequentially. (b) Resonance wavelength shifts (Δpm) from 3 separate microrings due to target miRNA (miR-24-1) and antibody (S9.6) infusion sequentially. (c) Responses of antibody (2 μg ml^{-1} S9.6) binding to the microrings having varied capture probe concentrations (from 16 nM to 20 μM) while the target miRNA concentrations were kept constant. (d) Data show the applicability of the suggested mechanism to multiplexed miRNA analysis. 2 target DNA functionalised chips were exposed to antibody solution following target infusion (miR-16 and miR-21). Only those having their complementary probe DNA and target miRNA showed a dramatic response due to the antibody infusion. Adapted from ref. 47 with permission.

densities following the miRNA infusions at the same concentration (40 nM). As shown in Fig. 17c, the elicited response due to antibody binding increased as the surface probe density increased. On the other hand, as the authors also indicated, after a certain surface probe density this increasing behaviour was not observed since possibly occurring steric effects due to probe crowding on the resonator surface resulted in a decrease in the antibody-binding rate.

Fig. 17d shows a multiplexed platform using this miRNA sensing approach. 2 different sensor arrays (Fig. 17d, each column) were infused by only 1 target miRNA-containing solution and only the microrings having DNA–RNA heteroduplexes elicited a response to the S9.6 infusion. The presented study demonstrates a simple miRNA sensing platform, which enabled real-time and multiple read-out measurements.

3.2 Messenger RNA (mRNA) detection

mRNA is a single-stranded RNA intermediate (between 500 and 10 000 bases), which possesses the complementary sequence of a DNA strand for representing a protein during the transcription process.[127] Studies have revealed a relationship between some mRNA expression levels (or mRNA abundance) and diseases,[128] *e.g.* in cancer types like colorectal,[129] prostate,[130] breast[131] and liver diseases.[132] Hence, as one of the transcriptomic biomarkers, detection of the mRNA molecules is quite critical for the diagnosis, treatment and determination of the stage of different types of diseases.[133–136]

So far, bulk mRNA detection has commonly been done *via* microarray[137–139] and real-time reverse transcription PCR (RT-PCR)[140,141] analyses. Also, a label-free cantilever-array sensor[142] was suggested as an mRNA detection platform. However, to detect cell-to-cell mRNA variations,[143] which can be observed in heterogeneous diseases like cancer, nanoflares[144] and core–shell nanocomposites[135] were used rather than the aforementioned bulk mRNA detection techniques, which were reported to be incapable of detecting the alterations.[135,144] In fixed or living cells, the mRNA levels were obtained using molecular beacons.[145,146] Withal, imaging of individual mRNA molecules in fixed cells was achieved using labelled probes.[147] In another study,[123] at the single cell level mRNA detection, the FISH technique combined with flow cytometry was used. Also, electrochemical-based biodetection techniques[148–151] can be used for the mRNA detection.

Several optical biodetection[152,153] techniques can provide rapid and label-free quantification of the mRNA molecules. As an optical detection technique, J. T. Kindt and co-workers[48] suggested silicon photonic microrings as optical microresonators for full-length mRNA quantification in a multiplexed manner with a 512 amol limit of mRNA detection. Likewise in previous works,[33,46,47] the S-4FB modified ssDNAs as probe molecules were tethered to the microring surface covalently. Also, the resonance wavelength shift was enhanced by adding short DNA chaperones and submicrometer beads, which improve hybridisation kinetics between the ssDNA probes and the target mRNA molecules.

3.3 Transfer messenger RNA (tmRNA) detection

tmRNA, which is a small molecule encoded by the *ssrA* gene[155] but is different from transfer RNA (tRNA) and ribosomal RNA (rRNA), was discovered in 1978 (ref. 154) as a new RNA component. This stable RNA piece can be found in many bacteria with a high copy number per cell, *Escherichia coli* being the most common example.[156–158] In all eubacteria and some eukaryotic organelles, tmRNAs play critical roles in translational surveillance and ribosome rescue to maintain the protein synthesis capacity of a cell.[157,159] The tmRNAs can be used as biomarkers in order to differentiate between bacterial species and genus, since each bacterial strain is known to contain unique regions of sequence.[49,158] Additionally, viable bacterial populations can be distinguished from non-viable ones using these biomarkers.[49,160]

Thus far, the tmRNA molecules were used as targets in conventional techniques for several detection purposes such as bacterial identification[158] or observing tmRNA localisation in bacteria[161] *via* fluorescence *in situ* hybridisation technique, and for pathogen detection using techniques based on nucleic acid sequence-based amplification,[162,163] real-time PCR,[155] real-time reverse transcription PCR (RT-PCR)[164] or surface plasmon resonance.[165]

Using photonic microcavities for tmRNA detection, O. Scheler and co-workers[49] discriminated the tmRNAs for different bacterial species. For this purpose, they fabricated chips having 32 individually addressed microrings integrated with a microfluidic assembly. An aryl aldehyde moiety having probes related to either *S. pneumoniae* or *S. agalactiae* bacteria was covalently conjugated to a reactive hydrazine group having microrings *via* hydrazone bonding. The fragmented tmRNA molecules were specifically detected *via* hybridisation with their probe DNA counterparts (Fig. 18a). However, in this technique, the detection of the tmRNA molecules required a pre-processing of the tmRNA samples *via* thermal tmRNA denaturation with/without a 10-fold excess of chaperones or by chemical tmRNA fragmentation, by which the secondary structures of the tmRNA molecules are disrupted. The obtained WGM shifts (pm) due to the sequential flow of different tmRNAs belonging to 4 bacteria, *K. pneumoniae*, *E. faecium*, *S. agalactiae*, and *S. pneumoniae*, are shown (Fig. 18b). The LOD obtained for this study was reported as 53 fmol *S. pneumoniae* tmRNA, which corresponds to approximately 3.16×10^7 CFU of bacteria. Although the suggested approach provided rapid and specific detections of different tmRNA species, as the authors also adverted to, the results showed a difference in terms of the WGM shift magnitudes, which was possibly observed due to undesired residual secondary structures of the tmRNA targets following the pre-process.

4. Protein detection using aptamers and DNA–antibody conjugates

The use of aptamers instead of antibodies is a recent approach in optical microresonator-based biosensing. The

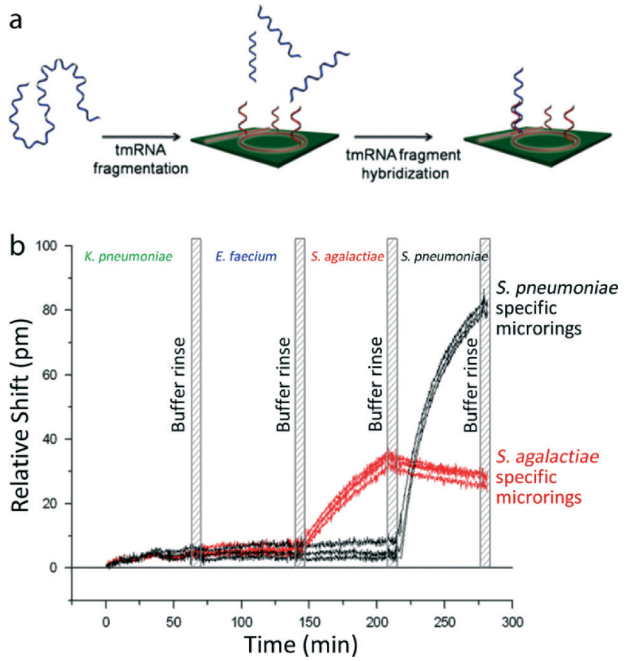

Fig. 18 Detecting different tmRNA species on a single chip with microrings integrated to a microfluidic assembly. (a) Schematic drawing shows their tmRNA detection approach in this work: the fragmented tmRNAs were hybridised with their probe counterparts attached to the microring surface. (b) Different tmRNAs from 4 bacteria, *Klebsiella pneumoniae*, *Enterococcus faecium*, *Streptococcus agalactiae*, and *Streptococcus pneumoniae*, were introduced sequentially to the flow chamber. Relative shifts (Δpm) from repeated experiments were obtained due to probe–target tmRNA hybridisation. Black and red data show response of the microrings having *S. pneumoniae* and *S. agalactiae* tmRNA specific DNA probes, respectively. In between each target infusion, washing with neat buffer solution was done. Adapted from ref. 49 with permission.

aptamers specifically recognise molecular patterns with high affinity. The main difference of the aptamers from protein-based antibodies is that they consist of nucleotides rather than amino acid chains, and they are synthesised artificially instead of being produced within living organisms.[166] Although they have more simple primary structures, *i.e.* smaller dimensions in terms of length and molecular weight,[167] the aptamers have successfully been demonstrated to have considerable affinity towards their targets, which are mostly proteins. Besides, they are more stable than their protein counterparts in terms of alterations in their environment and shelf life.[168] Their attachment to a silicon/silica surface is practically the same as in the oligonucleotide attachment strategies, which are well known,[169] and relatively easier than covalent binding of the antibodies. All the aforementioned factors make aptamers convenient for probing biological entities. Yet, their use in optical microresonator-based biodetection is not abundant. Although being quite promising, there are only a handful of examples regarding their use in this field. In our opinion, the rare use of the aptamers in optical microresonator-based biosensing is likely due to the possible difficulties encountered during the optical measurements, rather than the aptamers themselves, which was discussed previously within the text.

The earliest example related to optical aptasensors dates back to 2006, where Zhu and co-workers[50] demonstrated human thrombin detection using aptamer-conjugated microspheres.

The experimental set-up used in this work is shown in Fig. 19a. A fibre prism was used to couple light from a 980 nm tuneable laser source to a microsphere, while the laser was controlled *via* a computer DAQ card. They used 3-APS molecules to coat the microsphere surface *via* vapour deposition, and PDC as homobifunctional crosslinker to covalently attach amine-modified aptamers. The spectral response of the modified optical microsphere to the increased concentrations of thrombin (from 50 nM to 4.34 M) is given in Fig. 19b. Each increased spectral response showed a binding event that occurred between the aptamer and thrombin conjugates. However, after injection of 3.2 M thrombin, slower responses were obtained, most probably due to almost complete probe saturation on the microsphere surface caused by the infused high target concentration. They also reported a sensitivity of 1 NIH unit per ml, which corresponded to a concentration of 10 nM, limited by their spectral resolution of 0.2 pm. The corresponding data are shown in Fig. 19c.

The upper limit for a measurable dynamic range was reported as 5 μM. Yet, specificity seriously limited this dynamic range, particularly for thrombin, since the thrombin, with concentrations which were higher than 100 nM, was

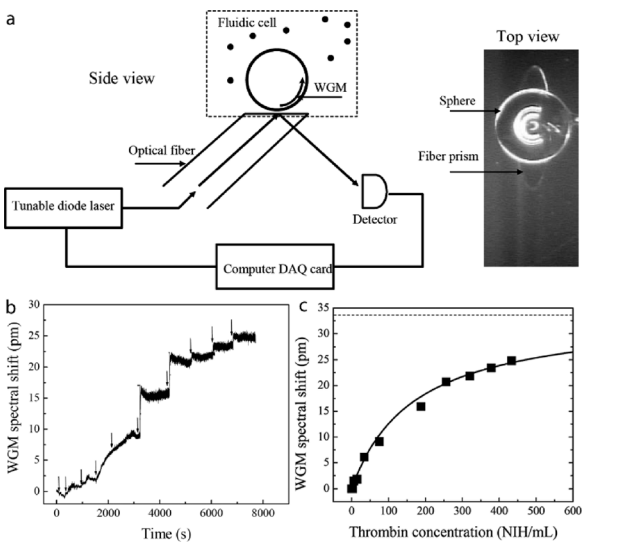

Fig. 19 Thrombin detection using an aptamer conjugated microsphere. (a) Experimental set-up (left). In a fluidic cell, the light from a tuneable diode laser (980 nm) is coupled to the microsphere *via* a fibre prism coupler (right). The laser was controlled using a computer data acquisition (DAQ) card. (b) Increasing concentrations of thrombin were applied and the WGM shifts (pm) were observed. The concentrations were 50 nM, 142 nM, 340 nM, 750 nM, 1.88 M, 2.56 M, 3.2 M, 3.786 M, and 4.34 M, beginning from the second arrow from the left. (c) The WGM shift (pm) regarding the thrombin concentration (NIH per ml) is given. 1 NIH unit corresponds to 10 nM. Adapted from ref. 50 with permission.

described as interacting with irrelevant aptamer probes. An arising electrostatic effect can be one of the reasons for such undesired interactions. Considering the fact that the isoelectric point of thrombin is high and thrombin is a cation at the pH of blood,[170] performing the experiment at pH ~7 can contribute to undesired interactions between the thrombin proteins and the irrelevant aptamers. The percentage of specific to non-specific binding interactions was calculated as 20% in concentrations higher than 500 nM (in phosphate buffered saline at pH 7.4). Moreover, the demonstrated substantial resistance of the aptamer-conjugated microspheres towards the BSA proteins could be another evidence of the aforementioned electrostatic effects. Also, considering the pH (~7) of the thrombin experiments, BSA is a quite suitable protein for investigating non-specific interactions occurring on a surface, since albumins are the most abundant proteins in blood. In addition, the BSA is negatively charged under the given experimental conditions, and since the aptamers also have a net negative charge, the occurring electrostatic repulsion can provide anti-fouling characteristics to the optical aptasensors.

Moreover, the optical coupling set-up used in this research utilises a fibre probe which was polished to form a prism at its end. This prism was used to couple light evanescently to the optical resonator. Although integration of high-Q factor microresonators like the microspheres with microfluidic systems is relatively challenging, this strategy can be further developed towards attaining this aim, resulting in a huge leap towards ultrasensitive optical biosensors integrated with lab-on-a-chip technologies.

A more recent example of the use of aptamers in combination with optical microresonators is the work of Park and co-workers.[51] Their detection scheme using anti-IgE aptamers is given in Fig. 20a. They performed multiplexed detection of IgE and human thrombin using APTES/GAD chemistry applied microring resonators having covalently attached aptamers. The detection limits reported for the IgE and human thrombin were 33 pM and 1.4 nM, respectively. The selectivity towards IgE was higher probably due to its larger dimensions. For a multiplexed detection, the optical microrings were functionalised individually.

Fig. 20b and c show the spectral shifts (pm) and the binding curve obtained at increasing IgE concentrations (from 67 pM to 0.67 nM), respectively. As can be concluded from Fig. 20b and c, the anti-IgE aptamer conjugated microrings showed considerable selectivity towards the IgE protein and similar responses with/without the presence of BSA proteins. The microrings functionalised to detect the thrombin proteins also showed resistance to the BSA molecules, likewise reported in the above work.[50] The dynamic range of the biodetection was given within a 4 orders of magnitude concentration difference. It was also mentioned by the authors that the biosensor could be reusable at least 10 times, using diluted sodium hydroxyl (NaOH) solution. In addition, a distinct advantage of using such a system is its suitability for microfluidic integration. In our opinion, this study is a frontier example of optical aptasensors, which have a potential to be developed especially for point-of-care applications.

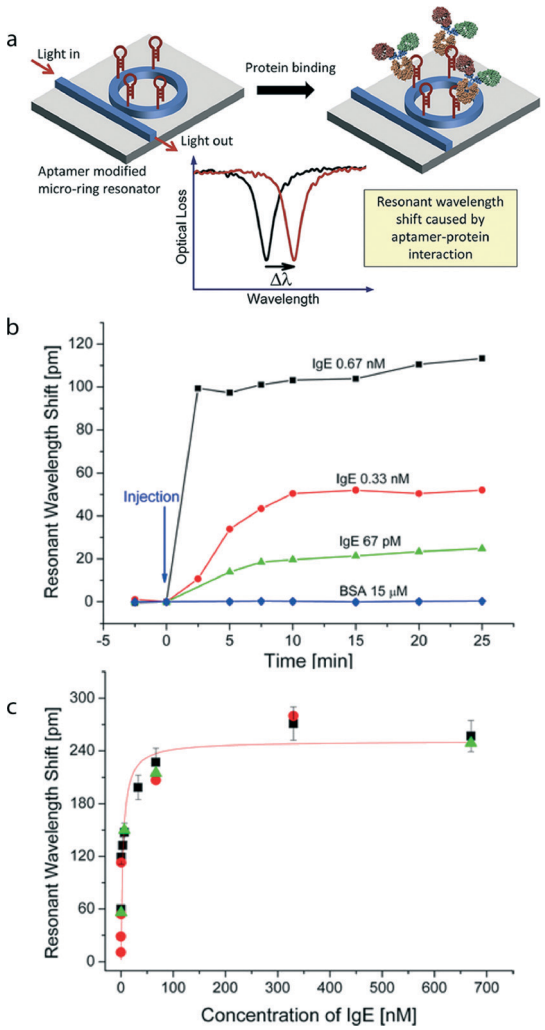

Fig. 20 Human immunoglobulin E (IgE) protein detection using optical microring aptasensors. (a) Once the aptamers are covalently attached to an optical microresonator surface, they can be stored for longer times compared to that of their antibody counterparts. The result of biorecognition is observed as a WGM shift ($\Delta\lambda$). Particularly, all on-chip systems, such as microring resonators coupled to their waveguides, can considerably benefit from the aptamers. (b) The spectral responses of anti-IgE aptamer conjugated microring resonators to injections of varied IgE concentrations (from 67 pM to 0.67 nM) and 15 μM bovine serum albumin (BSA) as control. (c) The binding curve for the varied IgE concentrations (nM). Black squares, green triangles and red circles show the results obtained by adding IgE solution continuously, one certain IgE concentration at a time in the presence of BSA and one at a time without the BSA, respectively. Adapted from ref. 51 with permission.

The last example regarding the optical aptasensors is the work of Pasquardini and co-workers[52] describing protein detections in complex media (human serum). They were able to detect thrombin concentrations less than 66 nM. The MPTMS-coated microspheres were functionalised with thiolated anti-thrombin aptamers (TBA) *via* disulfide chemistry. Light (773 nm) was coupled to the microresonator using a

tapered optical fibre. Fig. 21a shows the Q factors in air obtained from a microsphere after each surface modification step: cleaning (black line), MPTMS coating (red line) and covalent binding of the thrombins following TBA-15 aptamer probe conjugation (blue line). As can be seen from Fig. 21a, broadening in the spectral linewidth of the WGM was observed after each surface modification step due to a gradual increase in surface roughness of the microsphere, which is commonly encountered in surface modification of optical microresonators.

The inset in Fig. 21b shows confocal microscopy images of fluorescein (FAM) dye labelled TBA-15 (FAM-TBA-15) probes on a microsphere (green) and bound rhodamine dye labelled thrombins (red) on a TBA-15 probe conjugated microsphere. The authors showed that the TBA-15 conjugated optical aptasensor was particularly successful in detection in diluted human serum. The response of the biosensor towards thrombin in the diluted human serum (Fig. 21c) was identical to the response obtained in the buffer solution (Fig. 21b). Also, the biosensor did not show any response towards the BSA molecules, maintaining its specificity. The authors also showed reversible regeneration of the aptamers after biosensing several times. Although a minimum detectable limit was not provided, it can be deduced from the results to be less than 10 nM, similar to the above-mentioned work.[50]

Although there are only a few examples of aptamers regarding microresonator-based optical biosensing, they can be considered as useful probes in this field. However, the main concern regarding their application is specificity, which seems to be solved in the aforementioned work[52] to a great extent. Additionally, in all the discussed works, optical biodetection of the thrombin *via* aptasensors was performed. Although various types of aptamers are commercially available, studying the binding interactions between α-thrombin aptamers and thrombins *via* optical resonators is plausible, since they have been frequently used in diverse optical biodetection studies.[171,172] Though still more time is required for optical aptasensors to be common, there is yet an unprecedented potential regarding this field waiting to be explored and exploited. Especially, point of care applications integrated with microfluidic lab-on-a-chip systems could benefit from the durability of the aptamer probes substantially.

Lastly, as distinct from aptamer-based optical biosensing, A. L. Washburn and co-workers[53] suggested an alternative approach for optical microring-based antigen sensing. To increase the antigen binding capacity of the suggested system, they fabricated microrings with attached ssDNAs in arrays, and DNA–antibody conjugates having counterparts of the probe ssDNAs were hybridised on the microring surface. As the authors also indicated, using this approach provided practical DNA-based microring arrays for protein detection, which can be considered as more robust than only antibody-based ones in terms of stability and long-term durability under appropriate storage conditions. Additionally, the DNA–antibody conjugates offered self-assembled antibody arrays

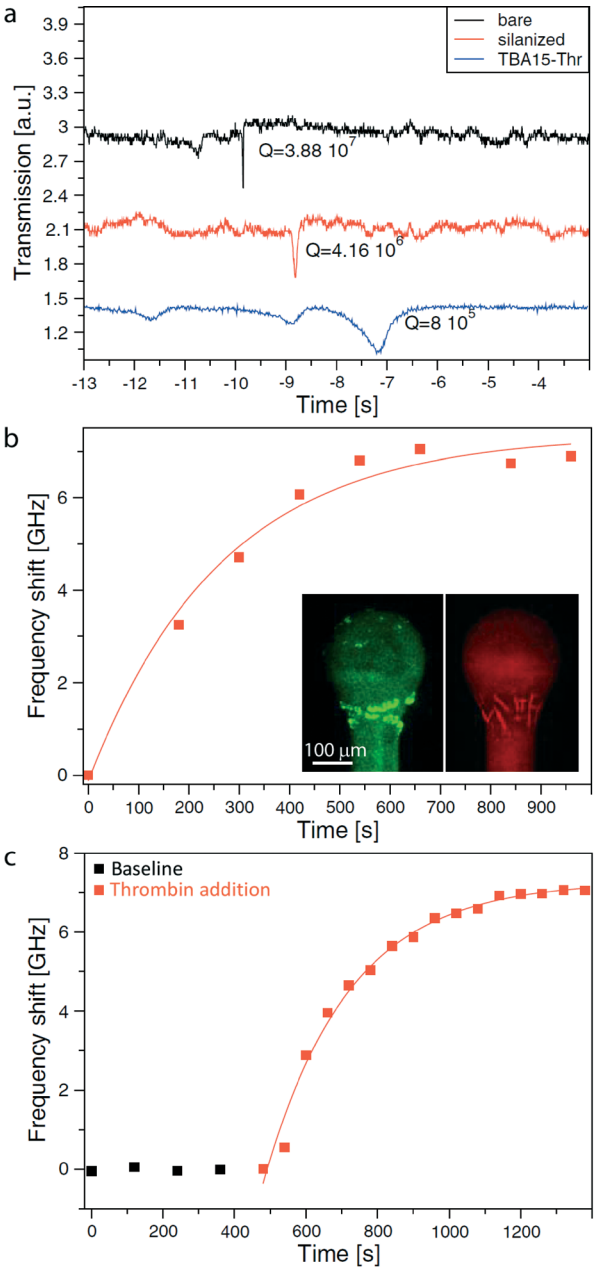

Fig. 21 Aptamer-based optical biosensing using microspheres in diluted human serum. (a) Measured Q factors (at 773 nm) of a bare (black line), the MPTMS-coated (red line) and the TBA-15 probe–thrombin conjugate (blue line) microsphere, respectively. (b) The response (GHz) of the TBA-15 conjugated microsphere towards thrombin in buffer is identical to (c) the response (GHz) in diluted human serum. This shows the biosensing capability of the aptasensor in a complex medium. Inset: Confocal microscopy images of the FAM-TBA-15 probes (green) and the rhodamine dye labelled thrombins (red) on a microsphere. Adapted from ref. 52 with permission.

(Fig. 22a) with a reduced steric hindrance, which plays a vital role in enhancing the antigen binding kinetics.[34,173,174]

Fig. 22b shows the slopes of spectral responses (Δpm) arising from 1 μg ml^{-1} prostate specific antigen (PSA) binding onto the modified microring surface using the DNA–antibody conjugates (F′-anti-PSA-5A6s, black squares) and antibodies

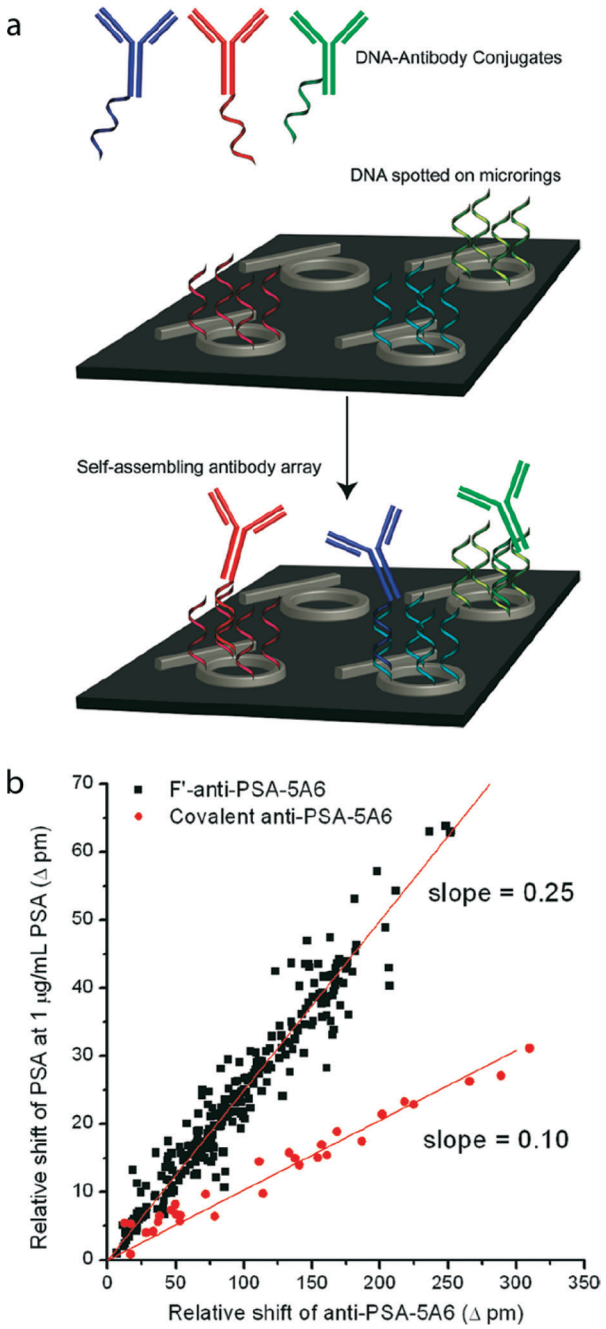

Fig. 22 Self-assembled DNA–antibody conjugates in microring arrays for prostate specific antigen (PSA) detection. (a) Schematic drawing showing how probe ssDNAs (red, blue and green strands) previously spotted on the microrings form DNA duplexes with the corresponding DNA–antibody conjugates, which have their counterparts. (b) The graph shows the increase (from 0.10 to 0.25) in the slope of the relative shift (Δpm) in the presence of the antibody–DNA conjugates. The PSA antigen (1 μg ml^{-1}) binding towards the DNA–antibody conjugates (F′-anti-PSA-5A6s, black squares) is 2.5 times greater than the result obtained by covalently bound surface antibodies (anti-PSA-5A6s, red circles). Adapted from ref. 53 with permission.

(anti-PSA-5A6s, red circles). The slope obtained by the F′-anti-PSA-5A6s (0.25) were 2.5 times higher than the slope obtained by using the anti-PSA-5A6s (0.10), proving the enhanced antigen sensing ability of the suggested antibody conjugation approach.

Future prospects

In this review, we have discussed various oligonucleotide-based applications of optical microresonators. All the works described here have one trait in common: they are all experimental works offering robust, reproducible and multiplexed detections; however, their implementations are not easily accessible yet. This does not necessarily mean that the WGM-type biosensors are inferior to their counterparts such as Surface Plasmon Resonance (SPR) biosensors because SPR-based biosensing for instance has a history dating back to at least 20 years compared to the WGM-type biosensors. Therefore, the production development regarding optimisation of the WGM-type biosensors could be considered as successfully accomplished only very recently. Yet, there are still a few major drawbacks on the side of optical microresonators as biosensors with robust operation. This last section is devoted to providing the general strategies that can be applied in order to enhance the applicability of the WGM type biosensors, anticipating their large-scale applications.

Material constraint is a critical point in biosensor technology. Although silicon and silica are relatively cheap materials, and chip scale production techniques are quite successful, plastics still constitute a considerably cheaper alternative, which is more suitable for mass production. A microfabricated optical microresonator can be utilised to form a mold, which then can be used to mass produce optical microresonators from plastics.[175] This means considering a new surface chemistry for bioconjugation as well, but there already exist versatile methods for chemically modifying plastics.[176]

There are also various other geometries of microresonators that have not been used for oligonucleotide-based biodetection. Microgoblets[177] and microbubbles[178] are two outstanding microresonator types that can be exploited for this purpose. Microgoblets are formed as polymer structures standing on silicon pillars, similar to microtoroids. They can be batch produced, and they can be used as microlasers by incorporating fluorescent molecules in their polymer. Laser is pumped by free space coupling, which is comparably easier than evanescent coupling, and the shift in the lasing wavelength could be monitored for biosensing.[177] Microbubbles, on the other hand, are structures similar to the OFFR resonators, but light is coupled to a bubble formed by arc discharge on the glass capillary. This enhances the Q factor by forming a trap for the travelling light. They could be functionalised in a manner similar to that of the OFFRs.[178]

Optical coupling of the WGM-type biosensors remain one of the greatest challenges. On-chip coupling of microtoroids[28] has been previously demonstrated in various studies and also described within this text. More robust methods for on-chip coupling of particularly the STIMs are quite critical regarding this aspect. This would enable an easy microfluidic integration, greatly enhancing the applicability of these biosensors.

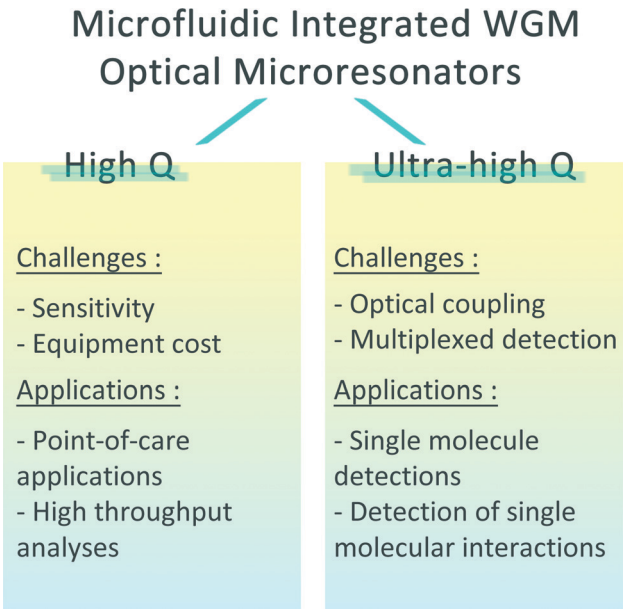

Fig. 23 Challenges and potential/current applications of the WGM-type optical microresonators. The diagram compares WGM-type microcavities having high and ultra-high *Q* factors.

Fig. 23 compares the challenges and potential/current applications of WGM optical microcavities. One serious problem related to optical biosensing using WGM microresonators is the expensive machinery behind it. Especially, tuneable lasers are costly research tools, and the whole system requires to be elaborately engineered during construction, operation, and maintenance. While current technology enables observation of extremely sharp resonances, tracking them for ultimate sensitivity also requires sensitive, thus expensive, devices. Therefore, a compromise should definitely be made. Point-of-care applications, for instance, do not necessarily require single molecule sensitivity; yet, increasing the shifts from the order of picometers towards nanometers could enable the tuneable lasers to be replaced with generic laser diodes. The miniaturisation of the system can go further if new laser sources can be developed by microresonators themselves. This could be attained by sensitivity enhancement techniques such as post recognition binding of bulky moieties,[48] or catalytic mass unloading.[32] Plasmonic enhancement could be exploited as well to increase the sensitivity of the microresonator towards perturbations in the medium.[23,179] In this way, detection could be performed by intensity interrogation, in a similar fashion to the SPR measurements by tracking the intensity at a fixed wavelength around the resonant wavelength[180] instead of the spectral shift, providing high-throughput analyses. On the other hand, single molecule detection experiments can help scientists to decipher many mysteries of life currently inaccessible with contemporary techniques. Single molecule binding events can be observed by using the WGM-type optical microresonators. The WGM biosensors are among the few tools that enable such a difficult task. For a reliable and reproducible experimental setup to be devised, the coupling problem should be seriously solved to a larger extent, enabling multiplexed detection.

Moreover, WGM resonators can provide various information about molecular orientations[181] and conformational changes,[182] since they support two orthogonal polarisations: the TE and TM modes. An electromagnetic wave at a certain polarisation can cause a shift both in the TE and in the TM modes since optical anisotropy in the refractive index occurs due to the preferred direction of self-assembled molecules adsorbed on the microresonator surface.[16] The aforementioned idea can be utilised to understand orientations and conformational changes of oligonucleotide molecules, self-assembled on a WGM resonator surface in a label-free manner.

Furthermore, surface engineering of the optical microresonators should seriously consider specificity as well as sensitivity. This applies whether an application is for a point-of-care detection or a single molecule measurement. There are recent examples of highly specific detections of oligonucleotides[34] as well as proteins.[26] Research in this field is promising when these results are considered.

In summary, optics possesses important possibilities regarding increasing the quality of our lives and extending our knowledge about the nano world. Referring to accurate questions would probably lead the scientific knowledge towards unprecedented answers, expanding our horizon.

Acknowledgements

PT would like to thank Ege Özgün for guiding scientific discussions on the manuscript. We also thank Ersin Hüseyinoğlu and Ozan Aktaş for critically reading the manuscript. This study was partly supported by the Scientific and Technological Research Council of Turkey (TUBITAK) with grant no 112 T612.

References

1 M. Baaske and F. Vollmer, *ChemPhysChem*, 2012, **13**, 427–436.
2 X. Guo, *J. Biophotonics*, 2012, **5**, 483–501.
3 G. J. Zhang and Y. Ning, *Anal. Chim. Acta*, 2012, **749**, 1–15.
4 J. Tamayo, P. M. Kosaka, J. J. Ruz, Á. S. Paulo and M. Calleja, *Chem. Soc. Rev.*, 2013, **42**, 1287–1311.
5 S. U. Senveli, Z. Ao, S. Rawal, R. H. Datar, R. J. Cote and O. Tigli, *Lab Chip*, 2016, **16**, 163–171.
6 T. Goda, K. Masuno, J. Nishida, N. Kosaka, T. Ochiya, A. Matsumoto and Y. Miyahara, *Chem. Commun.*, 2012, **48**, 11942–11944.
7 O. Avci, N. L. Ünlü, A. Y. Özkumur and M. S. Ünlü, *Sensors*, 2015, **15**, 17649–17665.
8 J. Haus, *Optical Sensors: Basics and Applications*, Wiley-VCH, Darmstadt, 2010.
9 F. S. Ligler and C. R. Taitt, *Optical Biosensors: Today and Tomorrow*, Elsevier, Hungary, 2008.

10 B. E. Rapp, F. J. Gruhl and K. Lange, *Anal. Bioanal. Chem.*, 2010, **398**, 2403–2412.
11 H. K. Hunt and A. M. Armani, *Nanoscale*, 2010, **2**, 1544–1559.
12 S. Mehrabani, A. J. Maker and A. M. Armani, *Sensors*, 2014, **14**, 5890–5928.
13 D. W. Kimmel, G. LeBlanc, M. E. Meschievitz and D. E. Cliffel, *Anal. Chem.*, 2012, **84**, 685–707.
14 J. R. Crowther, *ELISA: Theory and Practice*, Humana Press Inc., New Jersey, 1995.
15 C. Chen, Q. Xie, D. Yang, H. Xiao, Y. Fu, Y. Tan and S. Yao, *RSC Adv.*, 2013, **3**, 4473–4491.
16 F. Vollmer and S. Arnold, *Nat. Methods*, 2008, **5**, 591–596.
17 K. J. Vahala, *Nature*, 2003, **424**, 839–846.
18 M. J. Banuls, R. Puchades and A. Maquieira, *Anal. Chim. Acta*, 2013, **777**, 1–16.
19 T. A. Birks, J. C. Knight and T. E. Dimmick, *IEEE Photonics Technol. Lett.*, 2000, **12**, 182–183.
20 F. Vollmer, D. Braun, A. Libchaber, M. Khoshsima, I. Teraoka and S. Arnold, *Appl. Phys. Lett.*, 2002, **80**, 4057–4059.
21 M. S. Luchansky and R. C. Bailey, *Anal. Chem.*, 2012, **84**, 793–821.
22 I. Ament, J. Prasad, A. Henkel, S. Schmachtel and C. Sonnichsen, *Nano Lett.*, 2012, **12**, 1092–1095.
23 M. D. Baaske, M. R. Foreman and F. Vollmer, *Nat. Nanotechnol.*, 2014, **9**, 933–939.
24 T. J. Kippenberg, S. M. Spillane, B. Min and K. J. Vahala, *IEEE J. Sel. Top. Quantum Electron.*, 2004, **10**, 1219–1228.
25 S. Arnold, M. Khoshsima, I. Teraoka, S. Holler and F. Vollmer, *Opt. Lett.*, 2003, **28**, 272–274.
26 E. Ozgur, P. Toren, O. Aktas, E. Huseyinoglu and M. Bayindir, *Sci. Rep.*, 2015, **5**, 13173.
27 D. K. Armani, T. J. Kippenberg, S. M. Spillane and K. J. Vahala, *Nature*, 2003, **421**, 925–928.
28 X. Zhang and A. M. Armani, *Opt. Express*, 2013, **21**, 23592–23603.
29 D. W. Vernooy, V. S. Ilchenko, H. Mabuchi, E. W. Streed and H. J. Kimble, *Opt. Lett.*, 1998, **23**, 247–249.
30 F. Monifi, J. Friedlein, Ş. K. Özdemir and L. Yang, *J. Lightwave Technol.*, 2012, **30**, 3306–3315.
31 F. Vollmer, S. Arnold, D. Braun, I. Teraoka and A. Libchaber, *Biophys. J.*, 2003, **85**, 1974–1979.
32 Y. Wu, D. Y. Zhang, P. Yin and F. Vollmer, *Small*, 2014, **10**, 2067–2076.
33 A. J. Qavi, T. M. Mysz and R. C. Bailey, *Anal. Chem.*, 2011, **83**, 6827–6833.
34 P. Toren, E. Ozgur and M. Bayindir, *Anal. Chem.*, 2015, **87**, 10920–10926.
35 R. M. Hawk, M. V. Chistiakova and A. M. Armani, *Opt. Lett.*, 2013, **38**, 4690–4693.
36 J. D. Suter, I. M. White, H. Zhu, H. Shi, C. W. Caldwell and X. Fan, *Biosens. Bioelectron.*, 2008, **23**, 1003–1009.
37 Y. Shin, A. P. Perera and M. K. Park, *Sens. Actuators, B*, 2013, **178**, 200–206.
38 J. S. del Rio, T. Steylaerts, O. Y. F. Henry, P. Bienstman, T. Stakenborg, W. V. Roy and C. K. O'Sullivan, *Biosens. Bioelectron.*, 2015, **73**, 130–137.
39 Y. Shin, A. P. Perera, K. W. Kim and M. K. Park, *Lab Chip*, 2013, **13**, 2106–2114.
40 Y. Shin, A. P. Perera, J. S. Kee, J. Song, Q. Fang, G. Q. Lo and M. K. Park, *Sens. Actuators, B*, 2013, **177**, 404–411.
41 J. Yoon, M. K. Park, T. Y. Lee, Y. J. Yoon and Y. Shin, *Lab Chip*, 2015, **15**, 3530–3539.
42 T. Y. Lee, Y. Shin and M. K. Park, *Lab Chip*, 2014, **14**, 4220–4229.
43 R. M. Hawk and A. M. Armani, *Biosens. Bioelectron.*, 2015, **65**, 198–203.
44 J. D. Suter, D. J. Howard, H. Shi, C. W. Caldwell and X. Fan, *Biosens. Bioelectron.*, 2010, **26**, 1016–1020.
45 G. A. Rodriguez, S. Hu and S. M. Weiss, *Opt. Express*, 2015, **23**, 7111–7119.
46 A. J. Qavi and R. C. Bailey, *Angew. Chem., Int. Ed.*, 2010, **49**, 4608–4611.
47 A. J. Qavi, J. T. Kindt, M. A. Gleeson and R. C. Bailey, *Anal. Chem.*, 2011, **83**, 5949–5956.
48 J. T. Kindt and R. C. Bailey, *Anal. Chem.*, 2012, **84**, 8067–8074.
49 O. Scheler, J. T. Kindt, A. J. Qavi, L. Kaplinski, B. Glynn, T. Barry, A. Kurg and R. C. Bailey, *Biosens. Bioelectron.*, 2012, **36**, 56–61.
50 H. Zhu, J. D. Suter, I. M. White and X. Fan, *Sensors*, 2006, **6**, 785–795.
51 M. K. Park, J. S. Kee, J. Y. Quah, V. Netto, J. Song, Q. Fang, E. M. La Fosse and G. Q. Lo, *Sens. Actuators, B*, 2013, **176**, 552–559.
52 L. Pasquardini, S. Berneschi, A. Barucci, F. Cosi, R. Dallapiccola, M. Insinna, L. Lunelli, G. N. Conti, C. Pederzolli, S. Salvadori and S. Soria, *J. Biophotonics*, 2013, **6**, 178–187.
53 A. L. Washburn, J. Gomez and R. C. Bailey, *Anal. Chem.*, 2011, **83**, 3572–3580.
54 P. J. Gaffney and T. A. Edgell, *Thromb. Haemostasis*, 1995, **74**, 900–903.
55 J. D. Watson and F. H. C. Crick, *Nature*, 1953, **171**, 737–738.
56 R. Dawkins, *The Selfish Gene*, Oxford University Press, Oxford, 1976.
57 R. F. McClure, P. Kaur, E. Pagel, P. D. Ouillette, C. E. Holtegaard, C. L. Treptow and P. J. Kurtin, *Leukemia*, 2006, **20**, 176–179.
58 D. J. Lockhart and E. A. Winzeler, *Nature*, 2000, **405**, 827–836.
59 M. Byun, W. Han, B. Li, S. W. Hong, J. W. Cho, Q. Zou and Z. Lin, *Small*, 2011, **7**, 1641–1646.
60 L. G. Carrascosa, M. Moreno, M. Alvarez and L. M. Lechuga, *TrAC, Trends Anal. Chem.*, 2006, **25**, 196–206.
61 T. G. Drummond, M. G. Hill and J. K. Barton, *Nat. Biotechnol.*, 2003, **21**, 1192–1199.
62 J. Wang, *Anal. Chim. Acta*, 2002, **469**, 63–71.
63 Q. He, S. Wu, Z. Yin and H. Zhang, *Chem. Sci.*, 2012, **3**, 1764–1772.

64 G. Pelossof, R. Tel-Vered, X. Q. Liu and I. Willner, *Chem. – Eur. J.*, 2011, **17**, 8904–8912.
65 L. Matlock-Colangelo and A. J. Baeumner, *Lab Chip*, 2012, **12**, 2612–2620.
66 Z. Li, Y. Chen, X. Li, T. I. Kamins, K. Nauka and R. S. Williams, *Nano Lett.*, 2004, **4**, 245–247.
67 A. Ramachandran, S. Wang, J. Clarke, S. J. Ja, D. Goad, L. Wald, E. M. Flood, E. Knobbe, J. V. Hryniewicz, S. T. Chu, D. Gill, W. Chen, O. King and B. E. Little, *Biosens. Bioelectron.*, 2008, **23**, 939–944.
68 A. W. Peterson, L. K. Wolf and R. M. Georgiadis, *J. Am. Chem. Soc.*, 2002, **124**, 14601–14607.
69 M. S. Shchepinov, S. C. CaseGreen and E. M. Southern, *Nucleic Acids Res.*, 1997, **25**, 1155–1161.
70 V. R. Dantham, S. Holler, C. Barbre, D. Keng, V. Kolchenko and S. Arnold, *Nano Lett.*, 2013, **13**, 3347–3351.
71 S. Eustis and M. A. El-Sayed, *Chem. Soc. Rev.*, 2006, **35**, 209–217.
72 J. D. Suter and X. Fan, *Conf Proc IEEE Eng Med Biol Soc*, 2009, **2009**, 1042–1044.
73 E. Ozgur, P. Toren and M. Bayindir, *J. Mater. Chem. B*, 2014, **2**, 7118–7122.
74 K. B. Mullis, *Angew. Chem., Int. Ed. Engl.*, 1994, **33**, 1209–1213.
75 O. Piepenburg, C. H. Williams, D. L. Stemple and N. A. Armes, *PLoS Biol.*, 2006, **4**, 1115–1121.
76 S. Lutz, P. Weber, M. Focke, B. Faltin, J. Hoffmann, C. Muller, D. Mark, G. Roth, P. Munday, N. Armes, O. Piepenburg, R. Zengerle and F. von Stetten, *Lab Chip*, 2010, **10**, 887–893.
77 P. Singleton, *Dictionary of DNA and Genome Technology*, John Wiley & Sons, West Sussex, 2012.
78 H. Yan, R. Bonasio, D. F. Simola, J. Liebig, S. L. Berger, D. Reinberg and M. Berenbaum, *Annu. Rev. Entomol.*, 2015, **60**, 435–452.
79 J. Du, L. M. Johnson, S. E. Jacobsen and D. J. Patel, *Nat. Rev. Mol. Cell Biol.*, 2015, **16**, 519–532.
80 K. D. Robertson, *Nat. Rev. Genet.*, 2005, **6**, 597–610.
81 P. A. Jones and D. Takai, *Science*, 2001, **293**, 1068–1070.
82 P. A. Jones, *Nat. Rev. Genet.*, 2012, **13**, 484–492.
83 J. A. Law and S. E. Jacobsen, *Nat. Rev. Genet.*, 2010, **11**, 204–220.
84 L. Tan and Y. G. Shi, *Development*, 2012, **139**, 1895–1902.
85 S. Gopalakrishnan, B. O. Van Emburgh and K. D. Robertson, *Mutat. Res., Fundam. Mol. Mech. Mutagen.*, 2008, **647**, 30–38.
86 M. Tahiliani, K. P. Koh, Y. Shen, W. A. Pastor, H. Bandukwala, Y. Brudno, S. Agarwal, L. M. Iyer, D. R. Liu, L. Aravind and A. Rao, *Science*, 2009, **324**, 930–935.
87 N. W. Penn, R. Suwalski, C. O'Riley, K. Bojanowski and R. Yura, *Biochem. J.*, 1972, **126**, 781–790.
88 M. R. Branco, G. Ficz and W. Reik, *Nat. Rev. Genet.*, 2012, **13**, 7–13.
89 S. E. Cottrell, *Clin. Biochem.*, 2004, **37**, 595–604.
90 C. Bock, S. Reither, T. Mikeska, M. Paulsen, J. Walter and T. Lengauer, *Bioinformatics*, 2005, **21**, 4067–4068.
91 J. C. Susan, J. Harrison, C. L. Paul and M. Frommer, *Nucleic Acids Res.*, 1994, **22**, 2990–2997.
92 J. G. Herman, J. R. Graff, S. Myohanen, B. D. Nelkin and S. B. Baylin, *Proc. Natl. Acad. Sci. U. S. A.*, 1996, **93**, 9821–9826.
93 M. W. Y. Chan, L. W. Chan, N. L. S. Tang, J. H. M. Tong, K. W. Lo, T. L. Lee, H. Y. Cheung, W. S. Wong, P. S. F. Chan, F. M. M. Lai and K. F. To, *Clin. Cancer Res.*, 2002, **8**, 464–470.
94 M. Widschwendter, J. Berger, M. Hermann, H. M. Müller, A. Amberger, M. Zeschnigk, A. Widschwendter, B. Abendstein, A. G. Zeimet, G. Daxenbichler and C. Marth, *J. Natl. Cancer Inst.*, 2000, **92**, 826–832.
95 S. Zöchbauer-Müller, K. M. Fong, A. K. Virmani, J. Geradts, A. F. Gazdar and J. D. Minna, *Cancer Res.*, 2001, **61**, 249–255.
96 S. Bialik and A. Kimchi, *Semin. Cancer Biol.*, 2004, **14**, 283–294.
97 X. Tang, F. R. Khuri, J. J. Lee, B. L. Kemp, D. Liu, W. K. Hong and L. Mao, *J. Natl. Cancer Inst.*, 2000, **92**, 1511–1516.
98 F. van Roy, *Nat. Rev. Cancer*, 2014, **14**, 121–134.
99 C. H. Wang, H. C. Lai, T. M. Liou, K. F. Hsu, C. Y. Chou and G. B. Lee, *Microfluid. Nanofluid.*, 2013, **15**, 575–585.
100 M. F. Fraga and M. Esteller, *BioTechniques*, 2002, **33**, 632–649.
101 P. E. Nielsen, M. Egholm, R. H. Berg and O. Buchardt, *Science*, 1991, **254**, 1497–1500.
102 P. S. Ng and D. E. Bergstrom, *Nano Lett.*, 2005, **5**, 107–111.
103 M. I. Almeida, R. M. Reis and G. A. Calin, *Mutat. Res., Fundam. Mol. Mech. Mutagen.*, 2011, **717**, 1–8.
104 R. C. Lee, R. L. Feinbaum and V. Ambros, *Cell*, 1993, **75**, 843–854.
105 B. J. Reinhart, F. J. Slack, M. Basson, A. E. Pasquinelli, J. C. Bettinger, A. E. Rougvie, H. R. Horvitz and G. Ruvkun, *Nature*, 2000, **403**, 901–906.
106 N. C. Lau, L. P. Lim, E. G. Weinstein and D. P. Bartel, *Science*, 2001, **294**, 858–862.
107 K. Okamura, M. D. Phillips, D. M. Tyler, H. Duan, Y. T. Chou and E. C. Lai, *Nat. Struct. Mol. Biol.*, 2008, **15**, 354–363.
108 L. Vian, M. Di Carlo, E. Pelosi, F. Fazi, S. Santoro, A. M. Cerio, A. Boe, V. Rotilio, M. Billi, S. Racanicchi, U. Testa, F. Grignani and C. Nervi, *Cell Death Differ.*, 2014, **21**, 290–301.
109 A. Shenoy and R. H. Blelloch, *Nat. Rev. Mol. Cell Biol.*, 2014, **15**, 565–576.
110 Y. Zhang, W. Qin, L. Zhang, X. Wu, N. Du, Y. Hu, X. Li, N. Shen, D. Xiao, H. Zhang, Z. Li, Y. Zhang, H. Yang, F. Gao, Z. Du, C. Xu and B. Yang, *Sci. Rep.*, 2015, **5**, 09401.
111 X. Yan, Y. Huang, J. X. Zhao, C. J. Rogers, M. J. Zhu, S. P. Ford, P. W. Nathanielsz and M. Du, *Int. J. Obes.*, 2013, **37**, 568–575.
112 B. Xie, Q. Ding, H. Han and D. Wu, *Bioinformatics*, 2013, **29**, 638–644.
113 C. Guay and R. Regazzi, *Nat. Rev. Endocrinol.*, 2013, **9**, 513–521.
114 E. van Rooij and E. N. Olson, *Nat. Rev. Drug Discovery*, 2012, **11**, 860–872.

115 B. C. Richardson and D. R. Patel, *Nat. Rev. Rheumatol.*, 2014, **10**, 72–74.
116 L. Welberg, *Nat. Rev. Neurosci.*, 2015, **16**, 2–3.
117 V. A. Erdmann, S. Jurga and J. Barcizewski, *RNA and DNA Diagnostics*, Springer, Switzerland, 2015.
118 P. Landgraf, *et al.*, *Cell*, 2007, **129**, 1401–1414.
119 E. Várallyay, J. Burgyán and Z. Havelda, *Nat. Protoc.*, 2008, **3**, 190–196.
120 E. Curry, S. E. Ellis and S. L. Pratt, *Mol. Reprod. Dev.*, 2009, **76**, 218–219.
121 S. Roy, J. H. Soh and Z. Gao, *Lab Chip*, 2011, **11**, 1886–1894.
122 R. B. Schoch, M. Ronaghi and J. G. Santiago, *Lab Chip*, 2009, **9**, 2145–2152.
123 F. Porichis, M. G. Hart, M. Griesbeck, H. L. Everett, M. Hassan, A. E. Baxter, M. Lindqvist, S. M. Miller, D. Z. Soghoian, D. G. Kavanagh, S. Reynolds, B. Norris, S. K. Mordecai, Q. Nguyen, C. Lai and D. E. Kaufmann, *Nat. Commun.*, 2014, **5**, 5641.
124 B. N. Johnson and R. Mutharasan, *Analyst (Cambridge, U. K.)*, 2014, **139**, 1576–1588.
125 A. J. Qavi, J. T. Kindt and R. C. Bailey, *Anal. Bioanal. Chem.*, 2010, **398**, 2535–2549.
126 A. L. Washburn, L. C. Gunn and R. C. Bailey, *Anal. Chem.*, 2009, **81**, 9499–9506.
127 B. Lewin, *Genes VIII*, Pearson Prentice Hall, New Jersey, 2004.
128 F. W. Albert and L. Kruglyak, *Nat. Rev. Genet.*, 2015, **16**, 197–212.
129 M. Y. Kang, B. B. Lee, Y. H. Kim, D. K. Chang, S. K. Park, H. K. Chun, S. Y. Song, J. Park and D. H. Kim, *Int. J. Cancer*, 2007, **121**, 2192–2197.
130 D. M. Huffman, W. E. Grizzle, M. M. Bamman, J. S. Kim, I. A. Eltoum, A. Elgavish and T. R. Nagy, *Cancer Res.*, 2007, **67**, 6612–6618.
131 M. Braunstein, L. Liao, N. Lyttle, N. Lobo, K. J. Taylor, P. M. Krzyzanowski, I. Kalatskaya, C. Q. Yao, L. D. Stein, P. C. Boutros, C. J. Twelves, R. Marcellus, J. M. S. Bartlett and M. Spears, *Breast Cancer Res.*, 2016, **18**, 1–16.
132 A. Dropmann, *et al.*, *Oncotarget*, 2016, **7**, 19499–19518.
133 R. A. Sunde, *J. Nutr. Biochem.*, 2010, **21**, 665–670.
134 R. C. Gupta, *Biomarkers in Toxicology*, Elsevier, London, 2014.
135 L. S. Lin, Z. X. Cong, J. B. Cao, K. M. Ke, Q. L. Peng, J. Gao, H. H. Yang, G. Liu and X. Chen, *ACS Nano*, 2014, **8**, 3876–3883.
136 T. Chen, C. S. Wu, E. Jimenez, Z. Zhu, J. G. Dajac, M. You, D. Han, X. Zhang and W. Tan, *Angew. Chem., Int. Ed.*, 2013, **52**, 2012–2016.
137 P. O. Brown and D. Botstein, *Nat. Genet.*, 1999, **21**, 33–37.
138 J. Couzin, *Science*, 2006, **313**, 1559–1559.
139 J. J. Chen, *Pharmacogenomics J.*, 2007, **8**, 473–482.
140 T. Nolan, R. E. Hands and S. A. Bustin, *Nat. Protoc.*, 2006, **1**, 1559–1582.
141 H. D. VanGuilder, K. E. Vrana and W. M. Freeman, *BioTechniques*, 2008, **44**, 619–626.
142 J. Zhang, H. P. Lang, F. Huber, A. Bietsch, W. Grange, U. Certa, R. Mckendry, H. J. Güntherodt, M. Hegner and C. Gerber, *Nat. Nanotechnol.*, 2006, **1**, 214–220.
143 D. T. Ross, *et al.*, *Nat. Genet.*, 2000, **24**, 227–235.
144 A. E. Prigodich, P. S. Randeria, W. E. Briley, N. J. Kim, W. L. Daniel, D. A. Giljohann and C. A. Mirkin, *Anal. Chem.*, 2012, **84**, 2062–2066.
145 X. H. Peng, Z. H. Cao, J. T. Xia, G. W. Carlson, M. M. Lewis, W. C. Wood and L. Yang, *Cancer Res.*, 2005, **65**, 1909–1917.
146 P. J. Santangelo, B. Nix, A. Tsourkas and G. Bao, *Nucleic Acids Res.*, 2004, **32**, e57.
147 A. Raj, P. van den Bogaard, S. A. Rifkin, A. van Oudenaarden and S. Tyagi, *Nat. Methods*, 2008, **5**, 877–879.
148 A. C. Lee, Z. Dai, B. Chen, H. Wu, J. Wang, A. Zhang, L. Zhang, T. M. Lim and Y. Lin, *Anal. Chem.*, 2008, **80**, 9402–9410.
149 Z. Fang and S. O. Kelley, *Anal. Chem.*, 2009, **81**, 612–617.
150 X. Chen, S. Roy, Y. Peng and Z. Gao, *Anal. Chem.*, 2010, **82**, 5958–5964.
151 M. S. Wu, G. S. Qian, J. J. Xu and H. Y. Chen, *Anal. Chem.*, 2012, **84**, 5407–5414.
152 H. J. Lee, T. T. Goodrich and R. M. Corn, *Anal. Chem.*, 2001, **73**, 5525–5531.
153 T. K. Lim, M. Oyama, K. Ikebukuro and I. Karube, *Anal. Chem.*, 2000, **72**, 2856–2860.
154 S. Y. Lee, S. C. Bailey and D. Apirion, *J. Bacteriol.*, 1978, **133**, 1015–1023.
155 J. O' Grady, S. Sedano-Balbás, M. Maher, T. Smith and T. Barry, *Food Microbiol.*, 2008, **25**, 75–84.
156 B. Felden, H. Himeno, A. Muto, J. P. McCutcheon, J. F. Atkins and R. F. Gesteland, *RNA*, 1997, **3**, 89–103.
157 S. D. Moore and R. T. Sauer, *Annu. Rev. Biochem.*, 2007, **76**, 101–124.
158 W. Schönhuber, G. Le Bourhis, J. Tremblay, R. Amann and S. Kulakauskas, *BMC Microbiol.*, 2001, **1**, 20.
159 K. C. Keiler, *Nat. Rev. Microbiol.*, 2015, **13**, 285–297.
160 J. T. Keer, L. Birch and J. Microbiol, *Methods*, 2003, **53**, 175–183.
161 J. H. Russell and K. C. Keiler, *Proc. Natl. Acad. Sci. U. S. A.*, 2009, **106**, 16405–16409.
162 O. Scheler, L. Kaplinski, B. Glynn, P. Palta, S. Parkel, K. Toome, M. Maher, T. Barry, M. Remm and A. Kurg, *BMC Biotechnol.*, 2011, **11**, 1–7.
163 J. O'Grady, K. Lacey, B. Glynn, T. J. Smith, T. Barry and M. Maher, *FEMS Microbiol. Lett.*, 2009, **301**, 218–223.
164 S. McGuinness, T. Barry and J. O'Grady, *Food Res. Int.*, 2012, **45**, 989–992.
165 B. Glynn, K. Lacey, J. O'Grady, T. Barry, T. J. Smith and M. Maher, *J. Rapid Methods Autom. Microbiol.*, 2008, **16**, 210–221.
166 N. K. Navani and Y. F. Li, *Curr. Opin. Chem. Biol.*, 2006, **10**, 272–281.
167 A. Sassolas, L. J. Blum and B. D. Leca-Bouvier, *Biosens. Bioelectron.*, 2011, **26**, 3725–3736.
168 J. O. Lee, H. M. So, E. K. Jeon, H. Chang, K. Won and Y. H. Kim, *Anal. Bioanal. Chem.*, 2008, **390**, 1023–1032.

169 G. T. Hermanson, *Bioconjugate techniques*, Elsevier, Amsterdam, 2008.
170 W. Berg, B. Hillvärn, H. Arwin, M. Stenberg and I. Lundström, *Thromb. Haemostasis*, 1979, **42**, 972–982.
171 H. A. Ho and M. Leclerc, *J. Am. Chem. Soc.*, 2004, **126**, 1384–1387.
172 S. Song, L. Wang, J. Li, J. Zhao and C. Fan, *TrAC, Trends Anal. Chem.*, 2008, **27**, 108–117.
173 M. Stenberg and H. Nygren, *J. Immunol. Methods*, 1988, **113**, 3–15.
174 W. Kusnezow, Y. V. Syagailo, S. Ruffer, K. Klenin, W. Sebald, J. D. Hoheisel, C. Gauer and I. Goychuk, *Proteomics*, 2006, **6**, 794–803.
175 A. M. Armani, A. Srinivasan and K. J. Vahala, *Nano Lett.*, 2007, **7**, 1823–1826.
176 J. M. Goddard and J. H. Hotchkiss, *Prog. Polym. Sci.*, 2007, **32**, 698–725.
177 T. Wienhold, S. Kraemmer, S. F. Wondimu, T. Siegle, U. Bog, U. Weinzierl, S. Schmidt, H. Becker, H. Kalt, T. Mappes, S. Koeber and C. Koos, *Lab Chip*, 2015, **15**, 3800–3806.
178 A. Giannetti, A. Barucci, S. Berneschi, A. Cosci, F. Cosi, D. Farnesi, G. N. Conti, S. Pelli, S. Soria, S. Tombelli, C. Trono, G. C. Righini and F. Baldini, *Proc. SPIE*, 2015, **9506**, 950617.
179 S. I. Shopova, R. Rajmangal, S. Holler and S. Arnold, *Appl. Phys. Lett.*, 2011, **98**, 243104.
180 H. Nakagawa, I. Saito, T. Chinzei, Y. Nakaoki and Y. Iwata, *Sens. Actuators, B*, 2005, **108**, 772–777.
181 M. Noto, D. Keng, I. Teraoka and S. Arnold, *Biophys. J.*, 2007, **92**, 4466–4472.
182 J. Topolancik and F. Vollmer, *Biophys. J.*, 2007, **92**, 2223–2229.